eLife

Reviewed Preprint
v1 • April 17, 2026
Not revised

For correspondence:
ah687@sussex.ac.uk
yk348@sussex.ac.uk
l.lagnado@sussex.ac.uk

* These authors contributed equally.

Competing interests: No competing interests declared

Funding: See page 31

Reviewing editor: Megan R Carey, Champalimaud Foundation, Portugal

The Locomoting State Selectively Amplifies Activity of Sensitizing Neurons in Primary Visual Cortex

Antonio J Hinojosa[1,*], **Yehor Kosiachkin**[1,*], **Sina E Dominiak**[1], **Benjamin D Evans**[2], **Leon Lagnado**[1]

[1]Sussex Neuroscience, School of Life Sciences, University of Sussex, Brighton, United Kingdom • [2]AI Research Group, School of Engineering and Informatics, University of Sussex, Brighton, United Kingdom

eLife Assessment

This manuscript presents a **valuable** analysis of how locomotion modulates the activity of different subtypes of cortical neurons in the mouse primary visual cortex, showing that locomotion more strongly increases responses in sensitizing than in depressing excitatory cells. This data is then used to constrain a model of the responses. While the data are very interesting, the analyses remain **incomplete**, in particular due to concerns surrounding the modelling.

https://doi.org/10.7554/eLife.110088.1.sa4

Abstract

Sensory processing in the cortex reflects both adaptation to external stimuli and changes in internal state. To investigate how these processes interact in layer 2/3 of mouse V1 we combined calcium imaging, optogenetics and circuit modelling. We find that locomotion preferentially increases gain in pyramidal cells (PCs) that sensitize during visual stimulation compared to those that depress. A model explains this differential modulation through three mechanisms: (i) variations in the strength of PV and SST connectivity to individual PCs, (ii) broad locomotion-dependent weakening of PC and PV synapses, and (iii) reduced SST inhibition targeting sensitizing PCs. These results demonstrate that behavioural state selectively shifts cortical computation toward distinct adaptive regimes. The apparently paradoxical combination of increased PC gain but decreased synaptic strength is consistent with a state-dependent gating mechanism that boosts signals leaving V1 while simultaneously preventing disruption of the local excitatory-inhibitory balance required for stable computation.

Introduction

Sensory processing in the cortex is adjusted both by adaptation to the external environment and changes in the internal physiology of the animal associated with behavioural states such as attention, arousal and satiety[1–5]. The mechanisms by which external and internal variables interact within the cortical circuitry are not understood. Here we investigate this question by analyzing how the change in state associated with locomotor activity impacts adaptation in primary visual cortex (V1) of mice[6].

The dynamics of neurons in V1 reflect adaptation on multiple time-scales. In pyramidal cells (PCs), the initial excitatory response to an increase in contrast is followed by a fast (subsecond) decrease in gain reflecting depression in feedforward inputs from the LGN[7,8]. This is immediately followed by a slower phase of adaptation that varies dramatically across the PC population: while some PCs depress in response to a high-contrast stimulus others simultaneously *sensitize*[9]. PCs within layer 2/3 are not, therefore, a homogenous population: to understand gain control we must take into account variations in local inhibitory circuits in which they are embedded.

The onset of locomotion signals changes in internal state associated with attention or arousal, acting in less than a second to amplify visual responses in PCs[3,10–12]. A major driver of this increase in gain are cholinergic fibers arriving from the basal forebrain[2,13–15]. Some of these fibers make direct synaptic connections that excite interneurons expressing vasoactive intestinal peptide (VIP)[16], leading to amplification of PC responses through a VIP->SST->PC disinhibitory pathway. The majority of the cholinergic input, however, innervates V1 diffusely to modulate circuit function through extra-synaptic (muscarinic) receptors[2,13,16]. In vitro experiments have shown that M1 and M3 receptors on soma and dendrites of PCs can increase excitability while M2 receptors on axonal compartments reduce synaptic release probability[16–18]. Accounting for state-dependent changes in cortical processing therefore requires an integrated understanding of changes in both electrical activity and the strength of synaptic connections[12]. The difficulty is that modulations of synaptic strengths are very hard to quantify in awake and behaving animals: recording from connected neuron pairs remains technically challenging and is limited to anaesthetized animals in which inhibitory microcircuits are severely compromised[19–21]. Current understanding of synaptic modulation in cortical circuits is derived from *ex vivo* studies or inferred from indirect *in vivo* observations and modelling[12,22,23].

To understand how locomotion and adaptation interact in V1 of mice we used calcium imaging to record visual responses in PCs and the three major classes of interneuron (VIP, SST and PV) together with optogenetics to identify key interactions and a data-driven circuit model to estimate changes in synaptic weights. The model demonstrates that long-range inputs to VIPs that increase visual gain in the locomoting state also govern the time-course of adaptation over the behavioural time-scales of seconds. These inputs do not act uniformly across the PC population but preferentially increase the gain of neurons that sensitize to a high-contrast stimulus. Contrary to the prevailing model of gain control through the VIP->SST->PC pathway we find that visual responses in SSTs are not inhibited by locomotion but instead weakly enhanced. The model reconciles these observations through a neuromodulatory decrease in synaptic outputs across PCs and interneurons. Locomotion preferentially increases the gain of PCs that undergo the sensitizing form of adaptation because these receive a stronger SST connection than depressor PCs rendering them more sensitive to the weakening of SST synapses. These results provide an integrated view of the circuit mechanisms that adjust visual processing in V1 when an animal switches between resting and active states.

Results

Differential effects of locomotion on the fast and slow phases of adaptation

To understand how changes in brain state interact with adaptation in V1 we used two-photon calcium imaging to measure the activity of excitatory and inhibitory neurons in layer 2/3 during periods of rest and locomotion (Fig 1A, see Methods). The GCaMP6f signal in PCs responding to a high contrast stimulus (20° drifting grating at 1 Hz, 10 s duration) are shown in Fig. 1B. Locomotion increased the response averaged across all PCs by a factor of 2.2 ± 0.9. The dynamics of these responses varied widely between individual neurons; while some PCs responded with high initial gain and then depressed, others responded with low initial gain and then sensitized. This heterogeneity is illustrated by the raster plot in Fig. 1B which shows 522 neurons ordered by the time of peak activity: depression (early peak) and sensitization (late peak) were similarly represented in the two behavioural states (Fig 1B, top).

The increase in gain during locomotion was manifested in two ways; a 6-fold increase in the number of PCs generating a significant response (Supplementary Table 1) and an increase in the average amplitude of these responses measured as the integral during the 10 s stimulus (Fig. 1B). To investigate how these changes in gain affected PCs undergoing different forms of adaptation we split the population into three groups of equal size based on the distribution of a metric called the adaptive index (AI; Methods). These groups were sensitizing (AI less than zero), intermediate and depressing (AI more than zero; Fig. 1C). The AI, when computed separately for

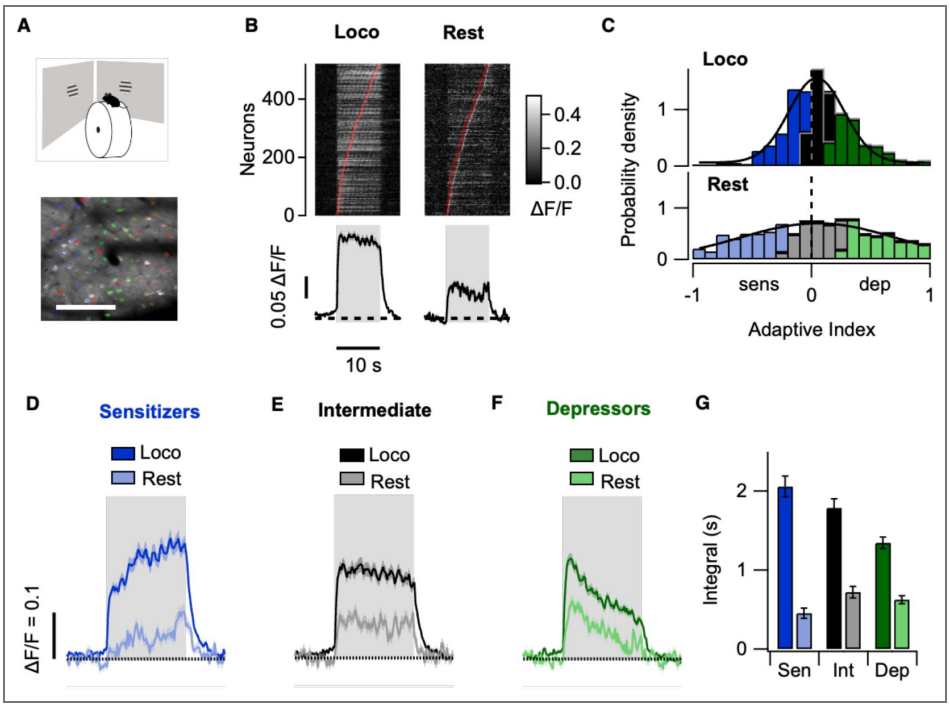

Figure 1. Slow adaptation in pyramidal cells during rest and locomotion.

A. Top: Mice running on a treadmill were shown a visual stimulus (drifting grating, 20° in size) for 10 seconds. Bottom: example field of view (FOV) showing PCs in V1 expressing GCaMP6f (grey) and corresponding regions-of-interest (ROIs) for individual neurons (rainbow). Scale bar represents 200 μm and stimulus lasts 10 s. **B.** Top: raster plots showing average calcium responses from individual PCs that were responsive to the stimulus during locomotion and rest (Same cells recordings between rest and locomotion, n = 522 neurons, from 9 mice, cells nested within animals). Responses are averaged over 10 stimulus trials then sorted by time of maximum amplitude in rest and locomotion independently. Bottom: average calcium response of all PCs to the visual stimulus during locomotion (left) and rest (right). **C.** Distributions of adaptive indices (AIs) in the PC population during locomotion (top) and rest (bottom) in sensitizers (blue), intermediate cells (grey) and depressors (green). Both distributions can be described by Gaussians with similar x_0 and different width (Rest, x_0 =0.001±0.9, width = 0.93±0.4; Loco, x_0 = -0.006±0.3, width = 0.33±0.02). **D, E, F.** Splitting the distribution of PCs according to their AI reveals that the tertile with lower AI showed slow sensitization, the tertile with intermediate values showed little adaptation, and the tertile with higher AI showed slow depression. **G.** Differences in gain of sensitizers (blue), intermediate cells (grey) and depressors (green) measured as the integral during the stimulus show that locomotion caused a stronger gain increase in sensitizers than in depressors ($p < 0.001$, Linear Mixed Model).

rest and locomotion and averaged across the whole PC population, was similar during locomotion (-0.006 ± 0.3; mean ± sem) and rest (0.001 ± 0.9; Fig. 1C) but the amplitude of the visual response increased by a factor of 4.5 ± 0.7 in sensitizing PCs, 2.5 ± 0.3 in intermediate group and 2.2 ± 0.2 in depressors. Locomotion therefore increased the gain of sensitizing PCs about twice as strongly as depressors (Fig. 1D-G).

Locomotion was associated with a second notable change in the dynamics of the PC population – a narrower distribution of adaptive effects (Fig. 1C). Cells that depressed at rest showed a shift towards sensitization, while cells that sensitized showed a shift towards depression (Supplementary Figure 1). Although this convergence may partly reflect differences in variability between states, the more uniform dynamics of adaptation parallels the increased temporal correlation observed across the PC population in behavioural states characterised by locomotion[24].

The immediate spiking response to a high-contrast stimulus is dominated by depressing adaptation[7,8] but the raw signal from calcium reporter proteins such as GCaMP does not easily distinguish this phase because of the gradual accumulation of calcium in the neuron. Several algorithms for estimating spike rates from calcium signals are now in use[25–27] and we applied MLspike because it is based on a biological model of GCaMP activation and calcium dynamics that has been shown to perform better than others[28] (Fig. 2-A-C). The first component of the spiking response was followed by fast depressing adaptation, as expected from electrophysiology[7,8,29] (red arrows In Fig. 2A-B). During locomotion, the initial peak amplitude was not significantly different in PCs that depressed (1.15 ± 0.08 Hz) or sensitized (1.11 ± 0.08 Hz), indicating similar strength of the feedforward input across the PC population (Fig. 2C).

Comparing activity at rest and while running revealed a powerful effect on both first and second phases of the response but this varied across the PC population. In the sensitizing tertile the initial peak driven by feedforward input underwent a relative increase of 2.1 ± 0.7 and the response integrated over the whole stimulus period a relative increase of 4.7 ± 1 (Fig. 2D). But in the depressing tertile, locomotion did not significantly change the initial fast response while the integrated response only increased by a factor of 1.4 ± 0.3 (Fig. 2E). Changes in internal state associated with locomotion do not, therefore, act uniformly across the PC population but preferentially increase the gain of neurons that undergo the sensitizing form of adaptation (Fig. 2F).

A data-driven model of contrast adaptation and the effects of locomotion

To understand how an active behavioural state differentially alters gain across PCs we constructed a population model of signal flow based on neuronal input-output functions expressed as firing rates[30–32] (see Methods). The model took into account three aspects of circuits in layer 2/3: *i)* the measured response dynamics of PCs and the three major types of interneurons (Fig. 2G-L); *ii)* the dynamics of signals that arrive from other brain regions (Fig. 3A), and *iii)* the known connectivity patterns of neurons within this layer (Fig. 3B). Code and example data sets are available at *https://github.com/lagnadoLab/CortexModel*.

i) The dynamics of neurons in layer 2/3

A key determinant of the magnitude and direction of slow adaptive changes in a PC is the local inhibitory microcircuit in which it is embedded: PCs in which direct SST inputs dominate over PV inputs tend to sensitize while those in which PV inputs dominate depress[9]. We therefore also experimentally measured the effects of locomotion on gain and adaptation in the three major interneuron types to use their response dynamics in the model (Fig. 2G-L). VIPs underwent the strongest modulation: the density of responsive neurons changed by a factor of 3 (Supplementary Table 1), and the integrated amplitude of these responses by a factor of 5.1 ± 1.0 (Fig. 2G). Simultaneously, locomotion caused the ratio of sensitizing (AI <0) to depressing (AI > 0) VIPs to increase from 1.3 at rest to 9 (Fig. 2J). PVs were more weakly modulated, with integrated responses changing by a factor of 1.7 ± 0.2 while the ratio of sensitizers to depressors also

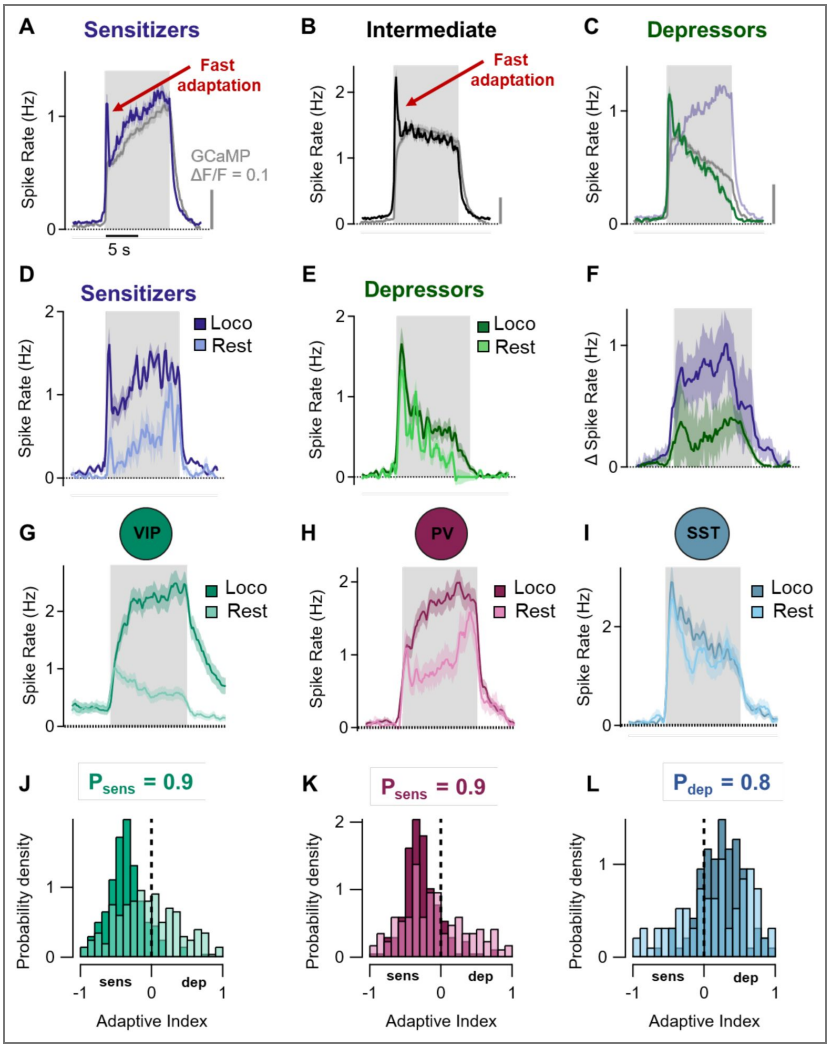

Figure 2. Differential effects of locomotion on fast and slow components of adaptation in PCs and interneurons.

A. Estimated spike rate averaged across all sensitizing PCs measured during locomotion (Data from all neurons responsive to the stimulus during locomotion including non-responsive cells during rest, n = 479 neurons from 14 mice). The GCaMP signal averaged across the same set of neurons is shown in grey. The fast depressing component of adaptation is highlighted by the red arrow. Stimulus duration 10 s. **B.** As A, but for the second (pre-dominantly non-adapting) tertile of PCs. **C.** As A, but for the depressing tertile. The trace from A is superimposed (light blue) showing the almost identical initial amplitude of the response in sensitizing and depressing PCs. **D.** Comparison of average spiking response at rest and during locomotion in the sensitizing tertile of PCs in which paired measurements were made (158 neurons in 9 mice). The relative change in the response during locomotion was 4.7 ± 1. **E.** Comparison of average spiking response at rest and during locomotion in the depressing tertile of PCs. The relative change in the response during locomotion was 1.4 ± 0.3 which was significantly smaller than the sensitizing tertile (T-test, $p < 0.001$). **F.** The time-varying difference in spike rate of sensitizing and depressing PCs. **G.** Average response of VIPs to the visual stimulus during locomotion and rest. The gain during locomotion increased by factor of 5.1 ± 1.0, measured from the integral of the responses. **H.** Average response of PVs to the visual stimulus during locomotion and rest. The gain during locomotion increased by factor of 1.7 ± 0.2. **I.** Average response of SSTs to the visual stimulus during locomotion and rest. SSTs showed a much smaller, nonsignificant, gain change 1.2 ± 0.2, p = 0.28. **J.** Distribution of adaptive indices in VIP interneurons (n = 122 neurons in 2 mice). Note that AI was measured from GCaMP signals, as for PCs in Fig. 1. VIPs were predominantly sensitizing. P_{sens} = 0.56 at rest and 0.90 during locomotion. **K.** Distribution of adaptive indices in PVs (n = 97 neurons in 3 mice). PVs were predominantly sensitizing. P_{sens} = 0.64 at rest and 0.86 during locomotion. **L.** Distribution of adaptive indices in SSTs (n = 82 neurons in 4 mice). SSTs were predominantly depressing at rest and during locomotion. P_{sens} = 0.37 at rest and 0.21 during locomotion. Results from D to L are from cell-paired recordings in the two states.

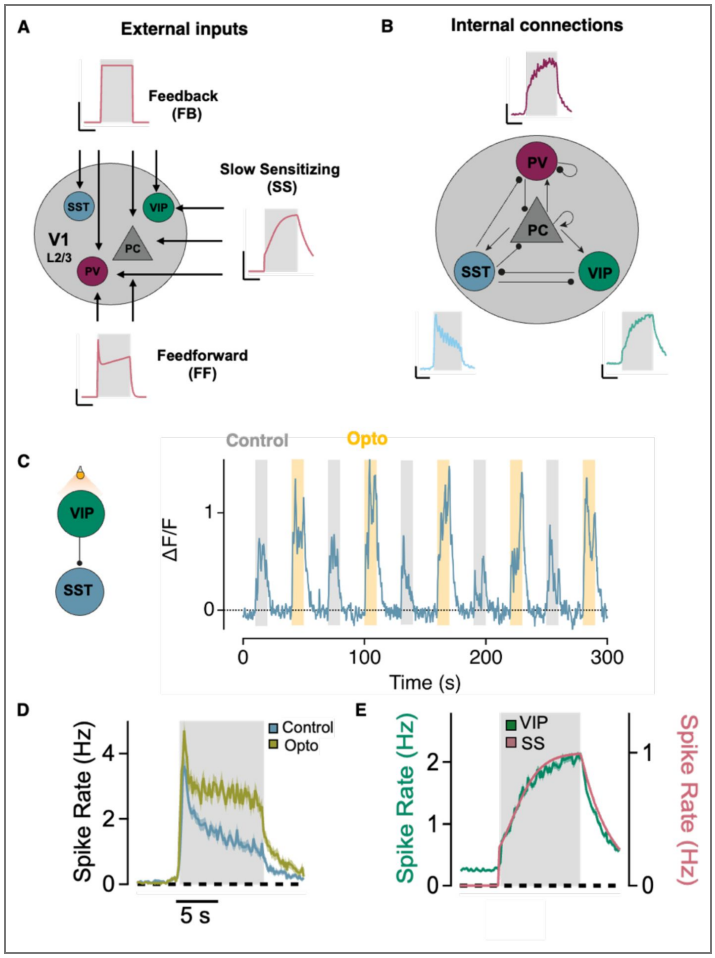

Figure 3. A model of signal flow in layer 2/3.

A. Schematic showing the targets of three external inputs into layer 2/3 of V1. Feedforward excitation targets PVs and PCs; feedback input targets all populations [50,51] and the slower sensitizing input enters through VIPs as well as directly activating PCs and PVs[52]. (Vertical bar: 0.5 Hz, horizontal bar: 5 s) **B.** Schematic showing the main excitatory (arrow tip) and inhibitory (round tip) connections between cell types within L2/3 of V1. PCs form excitatory connections with all other neuron types including themselves. PVs mainly target PCs and other PVs while SSTs inhibit all other cell types but avoid inhibiting each other. VIPs almost exclusively inhibit SST interneurons. (Vertical bar: 0.05 ΔF/F, horizontal bar: 5 s). **C.** Left: schematic showing the experimental paradigm to test if VIPs were a target for a slow sensitizing signal driving adaptation in layer 2/3: VIPs were silenced optogenetically while simultaneously recording activity in SSTs. Right: example response of an SST neuron during stimulus presentation alone and stimulus paired with optogenetic silencing of VIPs. **D.** Average response of SSTs with and without optogenetic silencing of VIPs (n = 83, from 4 mice). Silencing VIPs almost completely blocked slow adaptation. Light grey shade shows the stimulus time (10 s). **E.** The slow sensitizing input to the model (SS) was based on the average response of the VIP population during locomotion and consists of a step and sigmoid function with a time-constant = 1.71 s.

increased from 1.8 to 6.1 (Fig. 2H and K). In contrast, locomotion did not significantly alter the number of responsive SST neurons or the amplitude of their responses (gain factor of 1.2 ± 0.2; p = 0.28; Fig. 2I and L). This observation was surprising given that VIPs powerfully inhibit SSTs and locomotion activates a VIP->SST->PC disinhibitory pathway often highlighted as an important contributor to gain control[11,33,34]. However, the influence of this pathway is known to vary, consistent with reports that SST response to locomotion depend strongly on the visual stimulus[3,12]. A major aim of the model, therefore, was to take a more integrated view of gain control that considered multiple interacting pathways within layer 2/3.

The distribution of response dynamics in interneurons was more homogeneous than in PCs. The probabilities of a PC being sensitizing (AI <0, P_{sens}) or depressing (AI > 0, P_{dep}) were both ~0.5 (Fig. 1C), but during locomotion sensitization dominated in VIPs and PVs (P_{sens} = 0.9) while depression dominated in SSTs (P_{dep} = 0.8; Fig. 2J-L). These more consistent, cell-type-specific dynamics allowed us to represent each interneuron class by its characteristic average response (Fig. 2G-I), which we used as empirical input to a population mean-field model. Mean-field models have been widely used to describe the average behaviour of large populations of interacting neurons without simulating each neuron individually[30,35,36]. The network was represented by a system of four first order ordinary differential equations[30]:

$$\tau_i \frac{dr_i}{dt} = -r_i + f\left(\sum_j w_{ji} r_j + w_{in}\mathrm{In} + b_i\right) \quad (1)$$

where i, j are iterating through the four neuronal populations (PC, VIP, PV and SST), j is a presynaptic population and i postsynaptic, r is a firing rate and τ_i is the time-constant for that population. $f(x)$ is a neuronal input-output function and here we used a rectified power law[32]. The terms w_{in} In express the connection weights and amplitude of external inputs, and b_i the baseline activity of postsynaptic cell i. The connection weight between populations j and i, w_{ji}, is simply the product of the total number of synaptic connections, C_{ji}, and the average strength of an individual synapse between neuron type j and i, s_{ji}:

$$w_{ji} = C_{ji} s_{ji} \quad (2)$$

To compare the model to experiments, it was important to consider that not all presynaptic neurons are activated by the stimulus and, even if they are, they do not all activate the postsynaptic population because the connection probability (p_{ji}) is usually less than one. If, for instance, electrodes are placed on a PC and a nearby PV interneuron the probability of them being connected is only ~0.37 at distances less than ~150 µm while the average probability of an SST interneuron is even lower at ~0.27[37–39]. These factors can be taken into account by expanding relation 2 as

$$s_{ji} = {}^{w_{ji}}/_{N_j p_{ji}} \quad (3)$$

where N_j is the number of *responsive* presynaptic cells, defined as described in Methods. Below we infer changes in individual synaptic weights (s_{ji}) associated with a transition into the active state by comparing experimentally measured changes in N_j (Supplementary Table 1) to changes in connection weights (w_{ji}) estimated by fitting the model.

ii) The dynamics of signals entering layer 2/3

Excitatory signals entering layer 2/3 are of three main types[40,41]: feedforward (FF) drive originating from the lateral geniculate nucleus (LGN) and transmitted via layer 4, feedback from higher order cortices (FB)[42,43] and modulated inputs (SS), such as those gated by cholinergic

signals from the basal nuclei[11]. Electrophysiology has shown that FF inputs to layer 2/3 are dominated by fast depressing adaptation occurring within a few hundred milliseconds and the fast phase of adaptation in PCs fell within this range[7,8] (Fig. 2A-B). Calcium imaging *in vivo* has shown that drifting gratings lasting seconds can also generate a slower sensitizing component in FF inputs that enter layer 2/3 from layer 4[22,44]. The FF input was therefore modelled with both these components, as shown in Fig. 3A.

The second type of input to V1 is feedback from higher visual areas[45–47] and SST interneurons are one of their targets[46,48,49]. We have limited understanding of the dynamics of the FB signal over the time-scale of our stimulus, so, for simplicity, it was modelled as a step beginning at a delay of 380 ms after stimulus onset (Fig. 3A).

The third type of inputs to layer 2/3 are visually-activated signals that are strongly sensitizing in the locomoting state and drive slow sensitization. The dynamics of this signal were inferred from the visual response of VIPs measured experimentally during locomotion (Fig. 2G). We used these measurements because optogenetic experiments confirmed that activity in VIPs drove adaptation in downstream SST neurons, to which they are known to connect strongly[11,33,34] (Fig. 3C-D). To carry out this test we had to express the inhibitory photoprotein ArchT in VIPs and GCaMP6f in SSTs. Expressing different proteins in two interneuron populations was achieved by crossing a recombinant mouse line expressing Cre (VIP-Cre) with a Flippase expressing line (SST-Flp), then injecting two viral vectors that were Cre and Flippase dependent respectively (see Methods). Suppressing activity in VIPs almost completely abolished the slow component of adaptation in SSTs (Fig. 3D). Visually-driven inputs to VIPs include local recurrent excitation[33] and inputs from higher visual areas[53], and the combined dynamics of the later were modelled on the VIP response (Fig. 3E). This slow sensitizing signal appears quite distinct from inputs from the basal forebrain which provide a binary locomotion state signal but have been found *not* to respond to visual stimuli[54]. Notably, the dynamics of sensitization in VIPs were similar to sensitization in PCs suggesting that this input dominated slow adaptation throughout the network (Supplementary Figure 2).

iii) Connectivity within layer 2/3

Cortical connections have been probed using a number of approaches, including viral tracing[55], electrophysiology[33,37,39] and optogenetics[38], and we only considered connections that have been consistently observed in layer 2/3 and are strong enough to significantly influence the circuit (Fig. 3B). Not all neuron types connect; SST interneurons, for example, do not interact with each other while the very small number of connections from VIPs to PCs were neglected because these are not strong enough to significantly influence the circuit[33,38].

Using optogenetic manipulations to constrain model solutions and test its predictive ability

The model was fit to average populational responses of PCs and interneurons by adjusting the weights $w_{ji}$of external and internal connections in layer 2/3 (see Methods). Given the large parameter space spanned by the model, many solutions were of similar quality. Rather than identifying a single optimal solution, our fitting procedure revealed a region of parameter space that yielded good fits.

First, we generated 100,000 sets of evenly distributed initial parameters using Sobol sampling[22,56,57]. Of these, only 37 produced “good” solutions with chi-square < 10 in the locomotion condition, defining the approximate boundaries of the viable region. Next, this parameter subspace was explored further by local optimization using 20,000 Sobol initial conditions for each synaptic weight. This produced ~9000 good solutions in the locomotion condition with similar average and standard deviation to the initial 37. We then applied a third stage involving a series of experiments in which interneuron activity was altered optogenetically, which constrained the number of good solutions (to ~900) and the viable region of parameter space (Fig. 4). This third stage could not be usefully applied to data at rest because there were not enough recording episodes across all four optogenetic conditions and responses were smaller

and more variable than during locomotion[24]. We therefore limited the number of solutions by using a lower chi-square value of 3. The average parameter values after reducing the number of good solutions through all the steps are used to analyze the predictions of the model in Figs. 5 and 6.

The first optogenetic manipulation was to over-activate SSTs by expressing the excitatory photoprotein ChrimsonR using a Cre-dependent viral vector. Simultaneously, responses were recorded in PCs using GCaMP6f under the CaMKII promoter. The intensity of the photo-activating light was adjusted to increase the activity of SST interneurons by an average factor of ~2 in locomoting animals, as estimated in a separate series of experiments[9]. Fig. 4A (top) shows how the average PC response in the locomotion state was reduced compared to interleaved control trials.

Scaling the average SST activity within the model by a factor of 1.7 while leaving all other parameters constant provided an accurate description of the change in average PC activity in only 74% of the original ~9000 solutions (Fig. 4C). In other words, although a broad region of parameter space could reproduce the control data, introducing this optogenetic manipulation eliminated roughly one-quarter of the solutions, thereby narrowing the admissible parameter space.

After this first filtering step, we sequentially reduced the number of good solutions by constraining to results of SST silencing, PV activation and PV silencing, in this order. We found that while SST silencing and PV activation reduced the number of solutions to 25% and 11% of the original 9000, adding the last filter, PV silencing, had little further effect (Fig. 4C). Furthermore, connection weights remained identical when applying the first three optogenetic constraints compared to applying the fourth (Fig. 4D). PV silencing therefore served as a validation step: it confirmed the region of parameter space defined by the three previous filters instead of further refining it.

Locomotion increases PC gain but weakens their local synaptic output

Behavioural modulation of connection weights *within* layer 2/3 have been very hard to quantify experimentally, making it unclear how far changes in internal state adjust cortical processing through changes in neuronal activity as opposed to modulation of synaptic weights[14,16]. We used the model constrained by the four optogenetic manipulations to infer changes in synaptic weights. First, we investigated the action of locomotion averaged across the whole PC population (Fig. 5) and then explored why the subset of PCs that sensitize is modulated more strongly than those that depress (Fig. 6).

All the model solutions that allowed a good fit to the average visual responses in the four cell types closely followed both the fast and slow phases of adaptation at rest and during locomotion, as exemplified by the average solution (Fig. 5A-D, Supplementary Figure 3). Unsupervised clustering analysis identified a single cluster of solutions for locomotion and another for rest, indicating that these parameter sets form a continuum rather than falling into distinct categories. Moreover, examination of the distribution of each parameter revealed that all were unimodal, with no evidence for multiple peaks or clusters (data not shown). This pattern is consistent with gradual transitions within a single family of network configurations and supports the use of the mean as a representative summary. The average connection weights (Equation 2, w_{ij}) at rest are shown in the heatmaps in Fig. 5E and the relative changes with locomotion are summarized in Fig. 5F, calculated as:

$$\left[\mathrm{W}_{ij(loco)} - \mathrm{W}_{ij(rest)}\right] / \mathrm{W}_{ij(rest)} \tag{4}$$

Where free parameters predicted by the model could be compared with published experiment, there were several points of agreement. For instance, the relative strength of direct local connections to PCs were quantitatively similar to those measured using

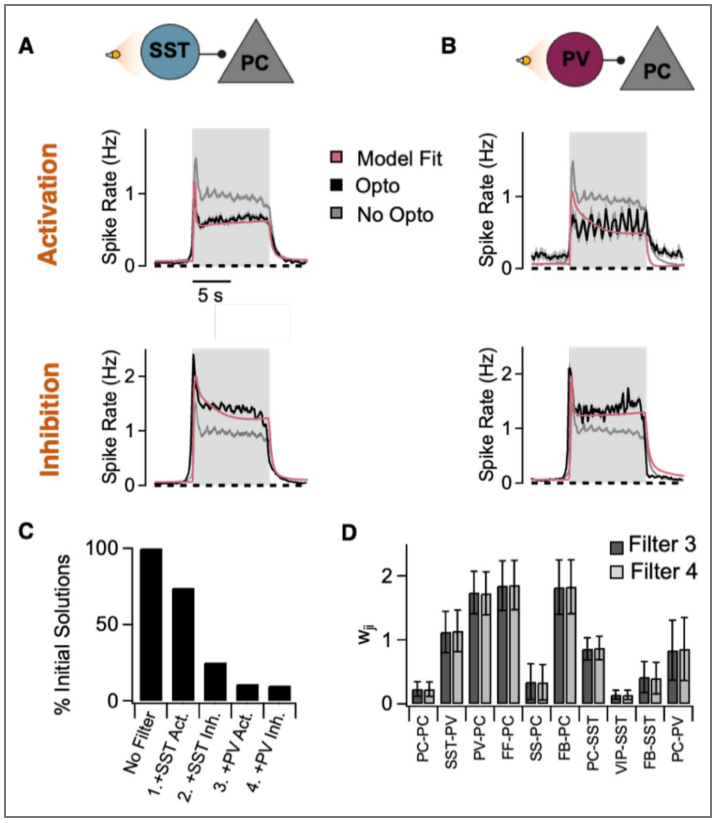

Fig. 4. Testing the model using optogenetics

A. Top: Average PC response with and without optogenetic activation of SSTs. Separate experiments indicated that this intensity of photoactivating light increased SST activity by a factor of ~1.7[9]. The red trace shows the model prediction when SST activity within the model was increased by the same factor. Activation of SSTs decreased PC gain and increased sensitization (top, RMSE = 0.27). The grey control trace (No Opto) is averaged over all four optogenetic conditions in A and B. Bottom: Average PC response with and without optogenetic inhibition of SSTs. Separate experiments indicated that this intensity of photoactivating light decreased SST activity by a factor of ~1.9[9]. The red trace shows the model prediction when SST activity within the model was decreased by the same factor. Silencing of SSTs resulted in an increase in gain and a shift to more depressing dynamics (bottom, RMSE = 0.31). **B.** Same as in C but when PVs were optogenetically activated (top, by a factor of ~2.5) or silenced (bottom, by a factor ~2.0) during stimulus presentations. Activation of PVs decreased the gain of PCs (top, RMSE = 0.32). Silencing of PVs resulted in an increase in gain and shift to more sensitizing dynamics (bottom, RMSE = 0.28). **C**. Proportion of the initial "good" solutions to the model (chi-square < 10) that also provided good solutions incorporating the results of the optogenetic manipulations in A and B. Filtering of solutions on the basis of adding optogenetic conditions was carried out in series in the order 1-4. Applying filter 4 (PV inhibition) had little further effect on the number of good solutions i.e almost all good solutions incorporating manipulations 1-3 also predicted the effects of PV inhibition. **D**. Comparison of connection weights (mean ± SD) of all good solutions after applying optogenetic filters 1-3 and 1-4. All weights remain similar after the fourth filter and it is these averages that are presented in Figs. 5 and 6.

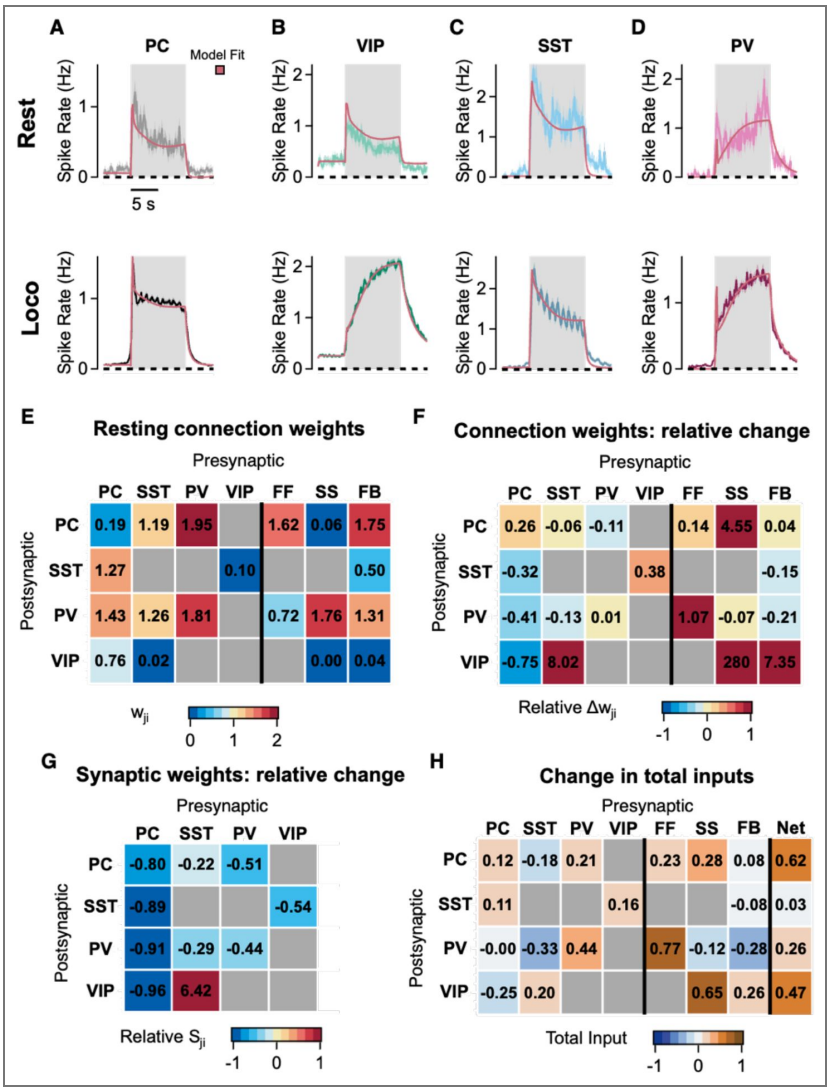

Figure 5. Locomotion modulates both electrical activity and the strength of synaptic connections.

A-D. Top: Average firing rates of PCs (A, black), VIPs (B, green), SSTs (C, blue) and PVs (D, dark red) during stimulus presentation at rest and their corresponding fits from the average of solutions calculated by the model (light red, RMSE = 0.19). Note that these traces show the average activity of only partially paired recordings, where only a subset of cells are matched between rest and locomotion (Rest n=158 from 9 mice, Locomotion n = 1437 neurons, from 14 mice). Bottom: average activity during locomotion in the same neuronal populations (RMSE = 0.11). **E.** Average resting connection weights from all solutions estimated by fitting the model to the activity of responsive neurons (Equation 2). **F.** The relative change in connection weights caused by locomotion (Equation 4). **G.** Relative change in synaptic weights based on estimated changes in connection weights **(F)** and measured changes in number of responsive cells (Supplementary Table 1; equation 3). Note that all excitatory and inhibitory synapses weaken except for synapses from SST to VIP which strengthen. **H.** The change in the total synaptic input activated by the stimulus, calculated from the average activity (Supplementary Table 2) and the change in connection weight in F (equation 5). The last column is the net change taking into account the polarity of the synapse.

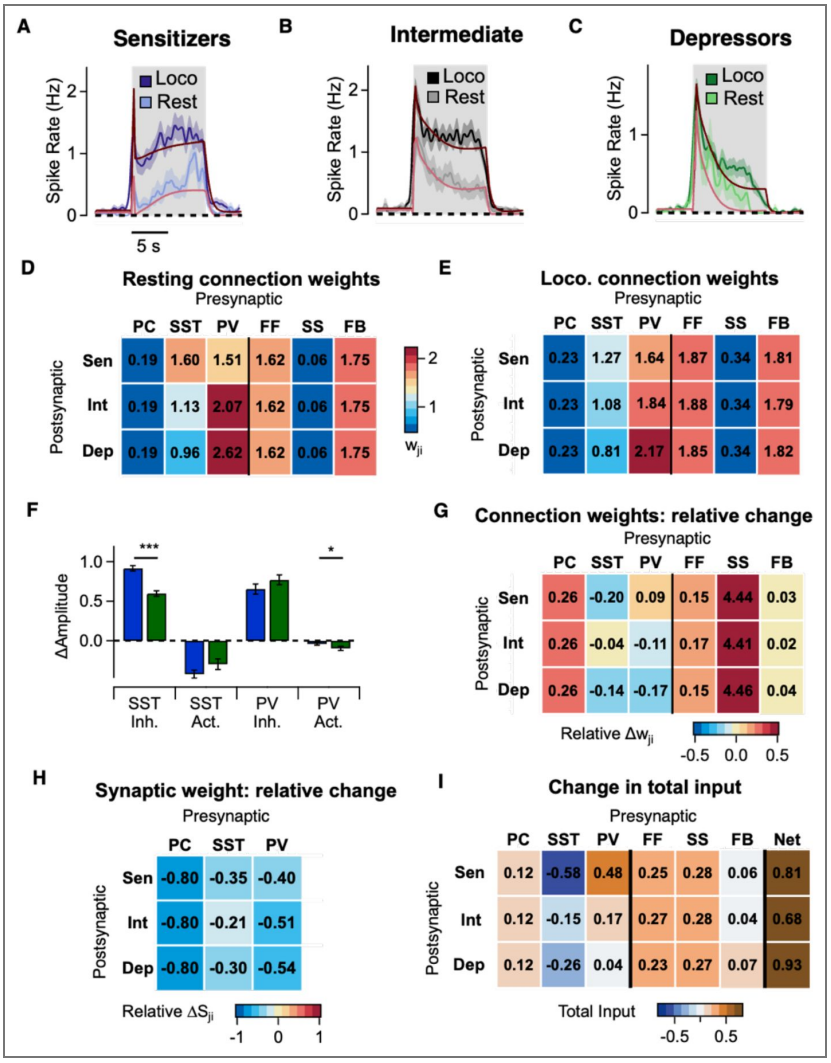

Figure 6. Differences in PV:SST input ratio determine the direction of PC adaptation and the change in gain associated with locomotion.

A. Activity of PCs from the tertile with lower AIs (sensitizers) at rest and during locomotion together with fits from the average of all good solutions calculated by the model (rest, RMSE = 0.22; loco, RMSE = 0.17). These are paired measurements from 158 neurons in 9 mice. During locomotion 7.5 ±1.2 more spikes were fired during the stimulus. **B-C.** As A, but for the intermediate and depressing tertiles, RMSEs were similar to sensitizers. During locomotion the stimulus generated 6.3 ± 0.9 more spikes in the intermediate group and 2.8 ± 0.4 in depressors. **D-E.** Heatmaps of the synaptic weights for each PC tertile at rest (D) and locomotion (E); sensitizers (Sen), intermediate (Int) and depressing (Dep). **F**. Amplitude change induced by optogenetic manipulation of SSTs and PVs in sensitizer (blue) and depressing (green) PCs. Note that sensitizers are preferentially modulated by SSTs and depressors by PVs as predicted by the model. (Inh: silencing with ArchT, Act: activation with ChrimsonR). **G**. Relative change in connection weights caused by locomotion for each subpopulation of PCs (calculated as equation 4). The key difference is the relative strength of PV and SST inputs. **H.** Relative change in synaptic weights caused by locomotion for each subpopulation of PCs. **I.** Change in total input during presentation of the stimulus received by each subpopulation of PCs. Sensitizers receive less SST inhibition than the intermediate and sensitizing tertiles. The last column shows the *net* change in total input, taking into account the polarity of the synapse.

electrophysiology[37,38]. There were, however, differences with other attempts to infer connection weights. Using our nomenclature, a recent modelling study[23] inferred a weight order in V1 at rest of $w_{PC\_PV} < w_{PC\_PC} < w_{PV\_PV} < w_{PV\_PC}$, while our results infer $w_{PC\_PC} < w_{PC\_PV} < w_{PV\_PV} < w_{PV\_PC}$ (Fig. 5E). This difference may reflect our models incorporation of long-range modulatory inputs, which also allowed it to predict other experimental observations, including a locomotion-dependent amplification of the slowly modulated input to VIPs[11] and PCs[52] and enhancement of feedforward drive to PCs[58,59]. The incorporation of long-range modulatory inputs into the model were essential to accurately estimating connection weights within layer 2/3 because removing these inputs did not yield any solutions following the same quality criteria (Supplementary Fig. 4, see Methods).

The model indicates that locomotion increases the gain of PCs through a broad combination of circuit effects but of particular importance is a 25-50% reduction in the strength of inhibitory synapses made by SSTs and PVs (Equation 3, s_{ij}; Fig. 5G). Strikingly, the model also predicts that the *total* weight of connections from PCs to all types of interneurons is decreased by one to three quarters following locomotion (Fig. 5F). The total synaptic input that neuron i receives from j, I_{ji}, is proportional to the activity of j and can be expressed as:

$$I_{ji} = w_{ji} r_j \tag{5}$$

Taking into account the 5-fold *increase* in the number of responsive PCs during locomotion (Supplementary Table 1) this leads to an estimated 90% decrease in synaptic strength across all PC targets (Fig. 5G). The model indicates that the large increase in PC and PV activity in the locomoting state is associate with a wide-spread decrease in the strength of their local synapses. This mechanism would allow large changes in the gain of signals *leaving* V1 for higher visual areas but without overexcitation of PC targets *within* the local circuit. The possible cholinergic mechanisms underlying these changes are considered in the Discussion.

In contrast to the rest of the local network, the average SST->VIP connection weight *increased*, by a factor of ~8 (Fig. 5F). The number of responsive SSTs neurons increased by only 22% (Supplementary Table 1) indicating that the major cause was a *strengthening* of SST synapses (Fig. 5G). This differential pattern on excitatory synapses of PCs (suppression) and SSTs contacting VIPs (enhancement) could be consistent with known variations in the distribution of different muscarinic acetylcholine receptors (see Discussion).

Switching to the active behavioural state also increased the strength of specific inputs to layer 2/3, most obviously the FF connections to PVs and the SS and FB connections to VIPs (Fig. 5F). VIPs were the most striking target, explaining their dramatic increase in gain (Fig. 2G).

Another way to summarize the effects of locomotion is to consider the change in the *total* synaptic input (both excitatory and inhibitory) as PCs respond to the visual stimulus (Supplementary Table 2; equation 5; Fig. 5H). The last column in Fig. 5H shows this change, taking into account the input received from all connected populations averaged over the stimulus presentation. The net excitatory input driving the visual response is more pronounced in PCs and VIPs compared to PV and SST interneurons, consistent with the locomotion-associated changes in gain shown in Fig. 2. Notably, the model predicted almost zero net change in total input to SSTs, consistent with the negligible change in SST activity observed experimentally (Fig. 2I) but inconsistent with the simple VIP->SST->PC disinhibitory model. The overarching picture is that locomotion adjusts the gain of visual responses by modulating both excitatory signals entering layer 2/3 and the strength of local synaptic connections, expanding what has been observed in a previous study[12].

Differential modulation of SST inputs onto sensitizing and depressing PCs

Why do some PCs sensitize while others depress? Optogenetic manipulations of interneurons indicate that the direction and amplitude of slow adaptation reflect the balance between PV and SST inputs[9]. PVs sensitize (Fig. 2H), so PCs in which these inputs dominate tend to depress, while SSTs depress (Fig. 2I), causing PCs in which these inputs dominate to sensitize. To make these ideas quantitative, we fit the model separately to the sensitizing, intermediate and depressing PC subpopulations (Fig. 6A-C). At rest, all the external connections to PCs had similar weights irrespective of adaptive properties; the stand-out differences were in the local inhibitory connections (Fig. 6D). In qualitative agreement with the "balance model", the direction of adaptation of a PC was dependent on the ratio of the PV and SST inputs, which increased progressively between the sensitizing, intermediate and depressing populations in both rest (0.9, 1.8 and 2.7, respectively; Fig. 6D) and locomotion (1.3, 1.7 and 2.7, respectively, Fig. 6E). We tested this prediction of the model by comparing the effect of optogenetic manipulations of SST and PV interneurons in the locomotion condition, confirming that sensitizers are more influenced by SSTs while depressors are dominated by PVs (Fig. 6F). This balance also influences the release from inhibition that different PCs undergo during locomotion, with sensitizers receiving less inhibition than depressors from SST interneurons, while the inverse pattern is observed for PV connections (Fig. 6G).

In principle, the differences in connectivity between sensitizing and depressing PCs could reflect synaptic strength. We found, however, only slight differences in the synaptic weight of all cell types connecting to PCs (Fig. 6H) and similar net total input between depressors and sensitizers (Fig. 6I). Again, the key difference was the SST:PV input ratio: sensitizers experienced a pronounced decrease in total SST inputs and increase in PV input (Fig. 6I). Notably, the increase in PC gain associated with locomotion did *not* correlate with changes in total inhibitory input (Fig. 6I), consistent with evidence that inhibition acts divisively rather than subtractively[60,61,62] (see Discussion). Overall, these results support the view that the enhanced gain observed in sensitizers is the result of their heightened exposure to a reduction in SST inhibition during locomotion.

Discussion

Adaptation is a fundamental aspect of sensory processing across cortical areas but it has not been clear how it is adjusted by changes in behavioural state that modulate these circuits. Here we have demonstrated that an active state acts on V1 to preferentially amplify responses in PCs that exhibit sensitizing adaptation over behavioural time-scales, with minimal effects on depressing PCs (Figs. 1 and 2). A data-driven network model indicates that locomotion modulates both the external inputs arriving to V1 and local synaptic connections. The differential modulation of the PC population reflects variations in their local inhibitory circuits: sensitizing PCs receive proportionally stronger SST input relative to PV input making them more susceptible to the locomotion-driven decrease in SST inhibitory strength (Fig. 6). More generally, these results build from the simple model of gain control through the VIP→SST→PC disinhibition pathway [11,63] by also considering the broader neuromodulatory actions of the cholinergic input to V1. The results, summarized in Fig. 7, indicate that locomotion increases the gain of PCs through a combination of circuit effects, including an increase in external inputs and a decrease in local inhibition (Figs. 5 and 6). We have not so far been able to identify other functions that correspond with sensitizing and depressing PCs: the initial gain of the visual response (Fig. 2C), receptive field location[9] and orientation tuning[9] are not significantly different between these groups.

Gating of the feedforward signal

The increase in gain during locomotion was profound: the number of PCs responding to the stimulus increased by a factor of six (Supplementary Table 1) and the average amplitude of those responses by a factor of 2-3 (Figs. 1 and 2). About 70–80% of PCs in layer 2/3 send axon

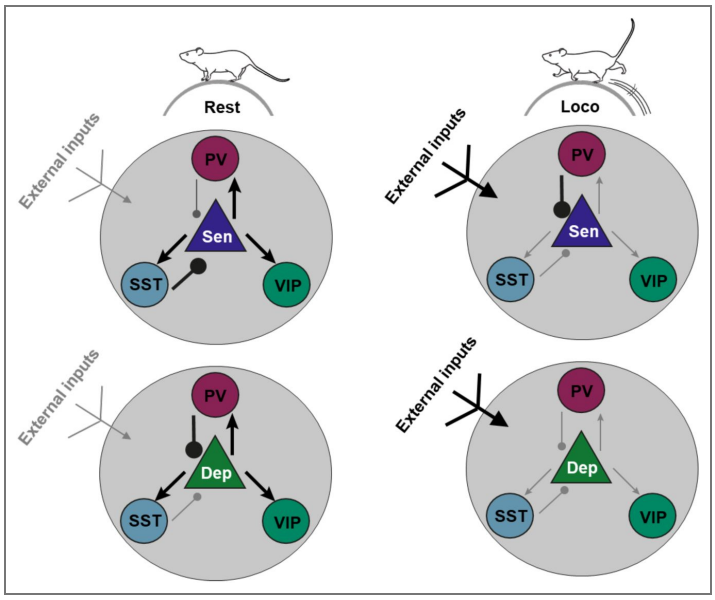

Figure 7. Summary of effect of locomotion in V1.

From rest (left) to locomotion (right) the connections from external inputs increase while the strength of PC connections to other targets is reduced. Sensitizers (top) receive stronger SST inhibition, being more sensitive to their reduction during locomotion, while depressors (bottom) receive stronger PV inhibition.

collaterals to higher visual areas[64,65] so these combined effects will strongly amplify the feedforward visual signal, at least to the drifting grating stimulus used here. The local recurrent signals are, however, strongly damped by a wide-spread decrease in the strength of recurrent PC synapses subject to local modulation (Fig. 5). This decoupling of spiking activity and synaptic efficacy suggests a mechanism by which V1 can amplify its output to downstream targets, such as higher visual areas, without generating excessive excitation in the local recurrent network. Such a mechanism could be important for maintaining the stability of computations that rely on balanced excitation and inhibition within V1. We suggest that the suppression of PC output reflects a gating mechanism that allows feedforward communication to be selectively boosted while shielding local circuits from saturation. This prediction could be tested by performing paired electrophysiological recordings of PC→PC connections during state transitions, but direct measurements of changes in synaptic strength in the cortex of behaving mice are currently extremely challenging - most of the available evidence is inferred from circuit-level activity patterns and *in vitro* studies.

Acetylcholine release triggered by activity in the basal forebrain and prefrontal cortex acts across large areas through volume transmission[15,66] but different muscarinic receptor types are expressed at specific locations, very often presynaptically, which provides spatiotemporally specific modulation[67]. The reduction in strength of local PC synapses during locomotion inferred from the model is in line with the known actions of acetylcholine on presynaptic M2 receptors, which reduce glutamate release at PC terminals[16–18]. Many cortical areas are subject to modulation through the cholinergic input that they receive [15,66], raising the possibility that signals from the basal forebrain also contribute to the increase in external input predicted by the model (Figure 5F).

Locomotion shapes cortical dynamics through multiple pathways

The first effect of locomotion was to enhance a slow sensitizing signal activated by the visual stimulus, the major target of which was VIP interneurons (Fig. 3). The source of this signal is likely the higher visual areas[43] gated by acetylcholine, and optogenetic experiments demonstrate that it determined the dynamics of adaption in SSTs (Fig. 3 and Supplementary Figure 2). The second major effect predicted by the model was an over 90% reduction in the strength of PC synapses across all targets (Fig. 5G), consistent with a range of evidence obtained *in vitro* demonstrating that M2 muscarinic receptors cause presynaptic inhibition[16,17,68]. A similar mechanism likely operates at PV, where release probability is reduced by M2 and M4 receptors[69–71]. However, the situation is different for SST interneurons. Our modelling shows that VIPs receive weak SST inputs at rest and that these synapses are *potentiated* during locomotion (Fig. 5E-G). This is likely to reflect a post-synaptic action of M1 receptors which have been shown to enhance postsynaptic $GABA_A$ currents in visual and somatosensory cortices[71,72]. In contrast, SST inputs to PCs and PVs appeared *weaker* during locomotion.

SSTs are a heterogenous class of inhibitory cells that target other cortical neurons in two distinct ways. The most numerous subtype, Martinotti cells, synapse on distal apical dendrites of PCs in layer 1 and show strong depressing adaptation, while Non-Martinotti cells generate more variable responses[48,73,74]. We suggest that SSTs contacting VIP interneurons are predominantly Non-Martinotti cells because they are the only subtype known to be enhanced by acetylcholine through M1 and M3 receptors *in vitro*[75]. It may also be that other neuromodulatory systems contribute to these mixed effects, including noradrenaline, serotonin and dopamine[2,11]. The models might be refined by splitting SSTs into two populations once their responses are measured separately[76], but a more critical next step is to test the predicted changes in synaptic strength. As for PC→PC connections, the best way to test this would be to make paired electrophysiological recordings of identified SST→PC and SST→VIP connections during state transitions.

A key insight from our modelling is that the relative strength of PV and SST inputs predicts both the direction of PC adaptation *and* the degree of locomotion-induced gain modulation (Fig. 6). Depressing PCs receive stronger PV input, consistent with their rapid and temporally precise inhibition[77]. In contrast, sensitizing PCs receive relatively stronger SST input which slowly depress to drive sensitization[9]. These differences in PV:SST ratio may also contribute to the changes in gain

associated with locomotion: because SST→PC inputs decrease substantially during locomotion (Fig. 5), PCs already dominated by SST input exhibit the largest gain enhancement. It is well established that there are substantial variations in the inhibitory input patterns to PCs but it is unclear how far these reflect the development of specific wiring patterns as opposed to the variability that will arise from random connections[37,78,79]. PV and SST interneurons are much sparser than PCs[80] and connect to them with low probabilities[37,39], such that simple random connectivity can give rise to PCs receiving different proportions of PV and SST inhibition – a pattern that at least partially occurs in V1[81].

Modulation of SST→PC inputs during changes in brain state

An intriguing prediction of our model is that the number of SST→PC synapses onto sensitizing PCs weaken whereas their PV→PC inputs increase selectively during locomotion (Fig. 6I). As a result of these opposing effects of inhibition, the total net input does not differ substantially from that of depressor PCs. There has been controversy regarding the computational form of SST and PV inhibition onto PCs: under certain experimental conditions SST inhibition has been described as subtractive and PV divisive[60], while different manipulations show the opposite[61,62]. Although in our model we initially considered both types of inhibition subtractive, one possibility is that SST interneurons induce divisive inhibition during rest, such that their effect strengthens disproportionately with increasing inhibition. This may therefore account for the marked gain increase we observed in sensitizer PCs, which receive stronger SST inhibition. In principle, this prediction could also be tested by targeted recordings of identified SST→PC connections during state transitions.

What are the consequences of the enhanced gain of sensitizing PCs during locomotion? One possibility is that these changes maintain responsiveness to low contrast and transient stimuli in a visual environment that has become more dynamic with a strong component of visual flow. By selectively enhancing PCs that resist rapid depression, the circuit may preserve sensitivity to behaviourally relevant stimuli[58,82]. From a computational perspective, the ability to differentially modulate adaptive subpopulations allows the cortex to tune its operating regime to changes in behaviour. Locomotion not only modulates the synaptic and gain mechanisms we focus on here but can also enhance neural representations of visual stimuli in V1[58]. Our findings might, therefore, also be interpreted in terms of broader theories of predictive coding and attention[83]: locomotion likely reflects an internal state of heightened predictive engagement with the environment and selective amplification of sensitizing PCs could in principle support enhanced cortical representations of expected sensory features.

Methods

Animal preparation

All experimental procedures in mice were conducted according to the UK Animals Scientific Procedures Act (1986). These were performed at University of Sussex under personal and project licenses granted by the Home Office following review by the Animal Welfare and Ethics Review Board.

The animals were housed in polypropylene cages (21 cm × 35 cm) that contained nesting material, a shelter, a treadmill, a tunnel and wooden sticks. Mice were housed in groups of 2 - 3, except in some instances when reintegration into a group was unsuccessful after surgery. All animals were kept on an inverted 12-hour light-dark cycle. Results are reported from four VIP-Cre mice (VIP tm1(cre)Zjh/J Jackson #010908), fourteen SST-Cre (SST tm2.1(cre)Zjh/J, Jackson #013044), four SST-Flp (Sst tm3.1(flpo)Zjh; Jackson #028579) x VIP-Cre and ten PV-Cre (Pvalb tm1(cre)Arbr/J, Jackson #008069), all of them adult mice aged from P90 to P260 from either sex. Mice were prepared for head-fixed multiphoton imaging through a surgical procedure in a stereotaxic frame under isoflurane anaesthesia. A titanium head plate was attached to the skull and a 3 mm craniotomy was drilled to expose the brain as described in detailed previously[9]. We then expressed AAV1.CaMKII.GCaMP6f.WPRE.SV40 to image calcium activity in pyramidal cells,

Key resources table.

REAGENT or RESOURCE	SOURCE	IDENTIFIER
Bacterial and virus strains		
AAV1	Addgene	100834
AAV1	Charité	VCA-222a
AAV5	Addgene	28305
AAV9	Addgene	100835, 62723
Experimental models: Organisms/strains		
VIP tm1(cre)Zjh/J	Jackson	#010908
SST tm2.1(cre)Zjh/J	Jackson	#013044
Pvalb tm1(cre)Arbr/J	Jackson	#008069
Sst tm3.1(flpo)Zjh	Jackson	#028579
Recombinant DNA		
AAV1.CaMKII.GCaMP6f.WPRE.SV40	Addgene	100834
AAV9.CAG.Flex.GCaMP6f.WPRE.SV40	Addgene	100835
AAV1.EF1a-FLEX(frt)-GCaMP6f-WPRE	Addgene	118273
rAAV9/Syn.Flex.ChrimsonR.tdTomato	Addgene	62723
AAV5.CBA.Flex.ArchT.tdTomato.WPRE.SV40	Addgene	28305
Software and algorithms		
ScanImage	MBF Bioscience	ScanImage v.5
PsychoPy	Peirce [84]	PsychoPy v. 1.82.02
IgorPro	Wavemetrics	IgorPro v.8
Suite2P	Pachitariu et al. [85]	MATLAB version
MATLAB	MathWorks, Inc	MATLAB 2021a
MLSpike	Deneux et al.[25]	MLSpike v.1.0
V1 Model	Laboratory of Leon Lagnado	https://github.com/lagnadoLab/CortexModel

AAV9.CAG.Flex.GCaMP6f.WPRE.SV40 to image interneurons in Cre lines and AAV1.EF1a-FLEX(frt)-GCaMP6f-WPRE to image SSTs in Flp lines. To excite interneurons optogenetically we used rAAV9/Syn.Flex.ChrimsonR.tdTomato and to inhibit them we used AAV5.CBA.Flex.ArchT.tdTomato.WPRE.SV40.

Multiphoton imaging *in vivo*

During imaging sessions mice were free to run on a cylindrical treadmill placed under a two-photon microscope, with stimuli being presented on two monitors covering most of the visual field. Visual stimuli were sinusoidal gratings drifting upwards (100% contrast, 1 Hz, 10 s duration) generated using the Python library PsychoPy[84]. The standard experimental protocol consisted of ten presentations of the stimulus with a 20 s interstimulus interval. When testing optogenetic manipulations these 10 trials were interleaved with 10 additional trials paired with illumination from an amber LED. The intensity of this LED was adjusted to activity of PCs to similar levels in different experiments. Running speed was measured with a rotary encoder and recorded through the imaging software (Scanimage5; Vidrio Technologies). The two-photon microscope (Scientifica SP1) employed a 16x water immersion objective (0.8 NA; Nikon) and imaging was carried out at a depth of 150-300 μm below the surface of the brain.

Raw movies were registered and segmented into regions of interest (ROIs) using the Suite2P package running in MATLAB 2021a[85] and further analysed using custom-written code in Igor Pro 8 (Wavemetrics). Here we only analyse results from the first imaging session in which the animal was exposed to the stimulus to avoid the effects of habituation observed over multiple sessions. Stimulus trials were only included for analysis if the mouse was running faster than 3 cm/s for more than 80% of the time. To calculate the response dynamics of PC, PV, SST and VIP populations we only included cells that were positively correlated with the stimulus. For each cell, the Pearson's correlation coefficients was computed between its activity trace (ΔF/F) and a stimulus trace binarized as either stimulus off (0) or stimulus on (1) using the StatsLinearCorrelationTest Function in IgorPro (Wavemetrics). The threshold for significant positive or negative correlation was set at $p < 0.05$. Measurements of adaptive properties were confined to cells which were significantly positively correlated with the stimulus. The adaptive index (AI) was calculated from the GCaMP6f signal as AI = (R1 − R2)/(R1 + R2) where R1 is the average response over the period 0.5 - 2.5 s after stimulus onset and R2 is the average at 8-10 s.

Estimation of firing rates

To estimate firing rates from the recorded ΔF/F data we used the MLspike algorithm using initial parameters expected for GCaMP6f[25]. Briefly, this finds the optimal spike train to fit the calcium fluorescence trace (ΔF/F) taking into account estimates of baseline fluorescence level and neuronal parameters including the amplitude of the unitary Ca^{2+} transient generated by a spike (A) and the decay time-constant of that transient (τ). These model parameters were obtained by maximum-likelihood autocalibration of ΔF/F traces, allowing conversion of relative fluorescence changes into inferred spike counts and corresponding firing rates.

In general, we followed recommendations and demos in the article and on the MLspike GitHub page. We set the range for A to be between 1 and 50% and τ was set at values from 0.05 to 3 seconds. The parameter A_{max}, which corresponds to the maximum amplitude of detected events, was 9, and the saturation parameter was set to 0.002. Finally, the Hill coefficient for Ca^{2+} binding to GCaMP6f was varied in the range from 1 to 3.75 with step sizes of 0.25.

Model of the circuit in layer 2/3 of V1

We built a rate-based data-driven population model of the network circuit in the mouse visual cortex layer 2/3 (code and example data sets at *https://github.com/lagnadoLab/CortexModel*). The purpose of the model was to understand adaptive gain control during rest and locomoting states of four main neuron populations (PC, PV, SST, and VIP). Model parameters, both fixed and fitted, are listed in Supplementary Table 3.

The network was represented by the system of four mean-field first order ordinary differential equations (equation 1)[30]. The neuronal input-output function, $f(x)$, was a rectified power law[32]

$$f(x) = k\left([x]_+^{\text{threshold}}\right)^n \tag{6}$$

where k is a scaling coefficient which was set to 1. This is a rectified linear function with a lower threshold, $[x]_+^{\text{threshold}}$, of zero to prevent negative values of firing rate and upper threshold of 25 to prevent run-away behaviour of the algorithm solving the network equations system. The exponent was set to n =2 but a linear activation function produced similar results during the fitting process, as observed by others[86].

Connectivity between and within populations is represented by total connection weight w_{ji}which is dependent on both the number of responsive cells in the presynaptic population and the strength of individual synapses. The number of presynaptic neurons responding to the stimulus varied between rest and locomotion so to assess changes in synaptic strength caused by neuromodulators the total connection weight was divided by the number of responsive presynaptic cells (Supplementary Table 1 and equations 2 and 3 in Results). The aim of fitting the model to the average activity traces of each neuronal population was to obtain connection weights, w_{ji}. Weights were set to zero where published work indicated that connections are very weak or non-existent, as between SST interneurons[33,38]. The final connection weights matrix for connections within layer 2/3 was represented as:

$$\begin{aligned} W &= \begin{pmatrix} w_{PC\_PC} & w_{PC\_PV} & w_{PC\_SST} & w_{PC\_VIP} \\ w_{PV} + PC & w_{PV\_PV} & w_{PV}SST & w_{PV\_VIP} \\ w_{SST\_}PC & w_{SST\_}PV & w_{SST\_}SST & w_{SST\_VIP} \\ w_{VIP\_PC} & w_{VIP\_PV} & w_{VIP\_SST} & w_{VIP\_VIP} \end{pmatrix} \\ &= \begin{pmatrix} w_{PC\_PC} & w_{PC\_PV} & w_{PC\_SST} & w_{PC\_VIP} \\ w_{PV\_PC} & w_{PV\_PV} & 0 & 0 \\ w_{SST\_PC} & w_{SST\_PV} & 0 & w_{SST\_VIP} \\ 0 & 0 & w_{VIP\_SST} & 0 \end{pmatrix} \end{aligned} \tag{7}$$

based on the reasonable assumption that connection probabilities are constant on the time-scale of minutes.

External inputs driving activity

Three types of external input drove activity in the circuit which we termed feedforward (FF), slow sensitization (SS) and feedback input (FB): the forms and origins of these are discussed in Results. These were represented in Equation 1 by the variable In that was specific for each input. The FF input was defined by the following system of equations:

$$In_{FF}(t) = \begin{cases} 0, & (t < s_{\text{start}} + s_{\text{del}}) \\ I_0 + A_f e^{-(t - s_{\text{start}} - s_{\text{del}})\lambda_f}, & (s_{\text{start}} + s_{\text{del}} + s_k > t \geq s_{\text{start}} + s_{\text{del}}) \\ I_0 + A_f e^{-(t - s_{\text{start}} - s_{\text{del}})\lambda_f} + k\left(t - s_{\text{start}} - s_{\text{del}} - s_k\right), & (s_{\text{start}} + s_{\text{dur}} \geq t \geq s_{\text{start}} + s_{\text{del}} + s_k) \\ \left(I_0 + A_f e^{-(s_{\text{dur}} - s_{\text{del}})\lambda_f} + k\left(s_{\text{dur}} - s_{\text{del}} - s_{\text{start}}\right)\right) e^{-(t - s_{\text{start}} - s_{\text{dur}})\text{decay}}, & (t > s_{\text{start}} + s_{\text{dur}}) \end{cases} \tag{8}$$

The initial short fast-depressing component had an amplitude A_f and decayed exponentially with a decay rate λ_f. The variables s_{start}, s_{del}, s_{dur}, s_k represent stimulus start, delay in the initiation of the response in a cell, the stimulus duration and an offset after the initial

peak, respectively. This offset defined the initiation of a second slow increase in feedforward input that has been observed in response to drifting gratings lasting seconds[22,44]. At the end of the stimulus presentation, experimental traces decayed relatively slowly compared with the time-constant of the model neurons and this was accounted for by including an exponentially decaying component to the input with the argument $decay_f$.

The temporal form of the feedforward input measured experimentally reflects the application of a spatio-temporal Gabor filter to a sinusoidal wave of drifting gratings[87]. This oscillation was clear in the activity of individual PCs but less evident in population averages because neurons responded with different phases, depending on the location of their receptive fields relative to the stimulus. This 1 Hz oscillation was most clearly observed in the average response of the SST population (Fig. 5C, bottom) which have larger receptive fields and therefore display less phase shifting[48]. We did not, therefore, attempt to model the oscillatory component of individual neuronal responses and concentrated on capturing the average activity across populations. The feedforward input (FF) was defined as a step of duration s_{dur} with initial amplitude ($I_5 + A_f$) which then decayed to a steady state of I_5 with time-constant 210 ms, defined by fitting the initial peak of the average PC response. The steady state was half the initial maximum with $A_f = I_5$. The linear increase is a simplified representation of the sensitizing behaviour observed experimentally in layer 4 activity[22,44].

The slow sensitizing input was represented by the following system of equations:

$$In_{SS}(t) = \begin{cases} 0 & ,(t < s_{\text{start}}) \\ \frac{A_s}{1+e^{(s_{\text{start}}+\text{del}-t)\lambda_s}} & ,s_{\text{start}} + s_{\text{dur}} \geq t \geq s_{\text{start}} \\ \frac{A_s e^{-(t-s_{\text{start}}-s dur^-)decay_s}}{1+e^{(\text{del}-s dur)\lambda_s}} & ,(t > s_{\text{start}} + s_{\text{dur}}) \end{cases} \quad (9)$$

where s_{start}, s_{dur} represent the time of the stimulus start and the stimulus duration, respectively. The slow sensitizing (SS) component is represented by a sigmoid function with an amplitude A_s, growth rate λ_s, and centre of sigmoid shifted to a del value from the stimulus starting time. Similarly to FF, the decay phase after the stimulus end was accounted for by the argument $decay_s$.

Finally, feedback input (FB) was represented by a step function:

$$In_{FB}(t) = \begin{cases} 0, & (t < s_{\text{start}} + s_{\text{fb}b_{\text{delay}}}) \cup (t > s_{\text{start}} + s_{\text{dur}}) \\ A_{\text{fb}}, & (s_{\text{start}} + s_{\text{dur}} \geq t \geq s_{\text{start}} + s_{\text{fb}b_{\text{delay}}}) \\ A_{\text{fb}} e^{-(t-s_{\text{start}}-s_{\text{dur}})\text{decay}_{\text{fb}}}, & (t > s_{\text{start}} + s_{\text{dur}}) \end{cases} \quad (10)$$

where s_{start}, s_{fb_delay}, s_{dur} represent time of the stimulus start, delay in the initiation of the response in a cell and the stimulus duration, respectively. The amplitude of the stimulus is defined by A_{fb}. Similarly to FF and SS, the decay phase after stimulus end was accounted for by the argument $decay_{fb}$. The amplitudes of A_{fb}, A_s and I_o were fixed around 1 Hz based on the average response of PCs during locomoting state (Fig. 2).

Fitting the model

To obtain values of connection weights we fit the model simultaneously to the average activity traces of the four neuronal populations using the *LMFIT* library in Python[88] by minimization of reduced chi-square parameter χ^2:

$$\begin{cases} \chi^2 = \sum_i^N \left(\text{data}_i - \text{model}_i\right)^2, & \text{eps is None} \\ \chi^2 = \sum_i^N \frac{\left(\text{data}_i - \text{model}_i\right)^2}{eps_i^2}, & \text{eps is not None} \end{cases} \quad (11)$$

Where ($data_i$ - $model_i$) represent an array of residuals between model and data points to be fitted, N – is the number of datapoints, and eps_i is the uncertainty of the data points. We weighted the data with uncertainty. We used standard errors from the locomotion and rest data.

$$\chi^2_{\text{reduced}} = \frac{\sum_i^N \left(\text{data}_i - \text{model}_i\right)^2}{\text{stderr}_i^2 \left(N - N_v\right)} = \frac{\chi^2}{\left(N - N_v\right)}, \quad (12)$$

Where N is the number of data points and N_v is the number of variable parameters. We set the threshold chi-square value to be 10 for locomotion and 3 for rest, given their different variabilities. An ideal "good fit" would have a value of reduced chi-square around 1, as far as uncertainty is provided[88]. We used standard errors of the mean (S.E.M) to weight the uncertainty of locomotion and rest data (eps). Additionally, to have a measure of fit quality independent of the data uncertainty and number of varied parameters we calculated root mean square error (RMSE) for each fit:

$$RMSE = \sqrt{\frac{\sum_i^N \left(\text{data}_i - \text{model}_i\right)^2}{N}}. \quad (13)$$

Parameter Search Strategy

Due to the high dimensionality of the parameter space, multiple parameter sets often produced similar χ^2_{reduced} values, indicating that networks with different connectivity profiles could generate similar activity patterns, which in turn made the results sensitive to the initial guess of parameters. While global optimization algorithms such as genetic algorithm and dual annealing were tested, they did not yield satisfactory performance for this model.

Instead, having access to the Artemis high performance computing cluster at Sussex University, we combined Sobol sampling[89] with local optimization methods. Sobol sampling provides uniform coverage of high-dimensional parameter space. We generated 100,000 sets of evenly distributed initial parameters and each Sobol-sampled parameter set was subsequently refined using local optimization. We tested *Levenberg-Marquardt, Nelder-Mead, Powell* and *L-BFGS-B* methods and noticed that *Nelder-Mead and Powell* performed across a broad parameter range, whereas *Levenberg-Marquardt* and *L-BFGS-B methods* were more effective for final fine-tuning. This two-stage procedure (global Sobol sampling of the initial parameters followed by local optimization) allowed us to systematically explore parameter space and quantify the variability of estimated connection weights. For the locomotion condition, we only obtained 37 solutions which were considered good fits for having chi-square lower than 10. In order to obtain more solutions for further filtering, we repeated the two-stage procedure limiting 20,000 Sobol initial conditions to a subspace to average ± 2SD for each synaptic weight, rendering 9,341 good solutions without changing the average and SD compared to the initial 37 solutions.

An important additional constraint was provided by requiring the model to fit the results of optogenetic manipulations of the PV and SST populations (Fig. 4), leading to a reduced number of sets of possible synaptic weights. In these experiments, the intensity of the LED was set to increase or decrease PV or SST activity by a known factor between 1.6 and 2.5, as measured empirically in other parallel experiments measuring GCaMP6f responses in these interneurons[9]. The average PV or SST activity trace was then scaled by the same factor for comparing the model to observed PC activity, and RMSE value calculated for each comparison in optogenetic tests. We

had a total of 4 conditions: SST activation, SST inhibition, PV activation and PV inhibition which we used for sequentially filtering the original group of solutions in 4 filtering steps. The threshold for a good opto fitting in each step was chi-square value smaller than 0.16 and 1.2 < OptoParam < 4. This approach allowed us to reduce the set of synaptic configurations, yielding parameter sets that captured both the average circuit dynamics during locomotion and the network's response to optogenetic perturbations.

For the resting state fits, we repeated the Sobol sampling and local fitting procedure using the same initial steps excluding optogenetic filtering, which allowed us to estimate mean parameter values and their variability (Supplementary Fig. 3). Optogenetic filtering was not feasible due to the noisier nature of these traces. Alternative versions of the model were tested by setting the connection weights of the tested connections to zero, this was performed with the SS and FB inputs. Notably, all the resulting solutions had chi-squared values above threshold indicating that slow sensitizing and feedback inputs are essential to explain circuit dynamics on these time-scales (Supplementary Figure 4).

To assess whether model parameters segregated into distinct groups, we applied unsupervised clustering using both K-means and DBSCAN algorithms. For K-means, we used the Elbow method and Silhouette analysis to estimate the optimal number of clusters. We further applied DBSCAN, estimating the neighborhood parameter (eps) from the 5th nearest neighbor distance using the KneeLocator method.

Fitting the model to subpopulations of pyramidal cells

The whole PC population was split into tertiles (sensitizers, intermediate cells and depressors) based on the distribution of adaptive index (Fig. 1). The average response of each subpopulation was then fit separately in for each of the good solutions from the locomoting and resting states using the two-stage fitting procedure explained above to assess changes in connectivity that describe the adaptive properties of each (Fig. 6). Three simplifying assumptions were made. First, that each subpopulation of PC receives the same shape of inputs as the average PC across the population. Second, only the synaptic weight of those connections directly targeting PCs were left free to vary while the other connections within the circuit were fixed. This was done because there is no change in activities of interneurons when separating a PC population into three subgroups and excitatory input from PCs to interneurons was taken as an average response of the whole PC population, similarly as during fitting of the whole network. Third, we used the initial conditions of the average models scaled to match amplitudes of subpopulations to average response. From Equations 1 and 6 the scaling factor is:

$$\text{scale} = \frac{w_{\text{tertile}}}{w_{\text{avg}}} = \sqrt{\frac{A_{\text{tertile}}}{A_{\text{avg}}}}, \tag{14}$$

where w_i is a weight and A_i is an average amplitude of response during stimulus.

Corresponding scaling multiplication factors for locomotion are: sensitizers = 1.1, intermediate = 1.2, depressors = 0.8, and for resting state are: sensitizers = 0.9, intermediate = 1.1, depressors = 0.9.

Statistical analysis

For the statistical tests not directly related with the model fitting we used the analytical software Igor Pro 8 and/or SPSS ('Statistical Package for the Social Sciences', IBM). To determine if the mean of one group was significantly different from another group we used a t-test (two-sided) if the distribution was normally distributed or a non-parametric Mann–Whitney U test (MWU) if it was not. We used linear mixed modelling (LMM) to test for significant interaction between locomotion state and AI tertile (Fig. 1), because cells were not paired between locomotion and resting states.

Locomotion state and AI tertile were defined as fixed variables and the animal ID was defined as the random variable. All values are given as as mean ± standard error of the mean (SEM) or mean ± standard deviation (SD) as indicated in each figure legend.

Supplementary Information

Locomotion-dependent changes in adaptive properties of PCs

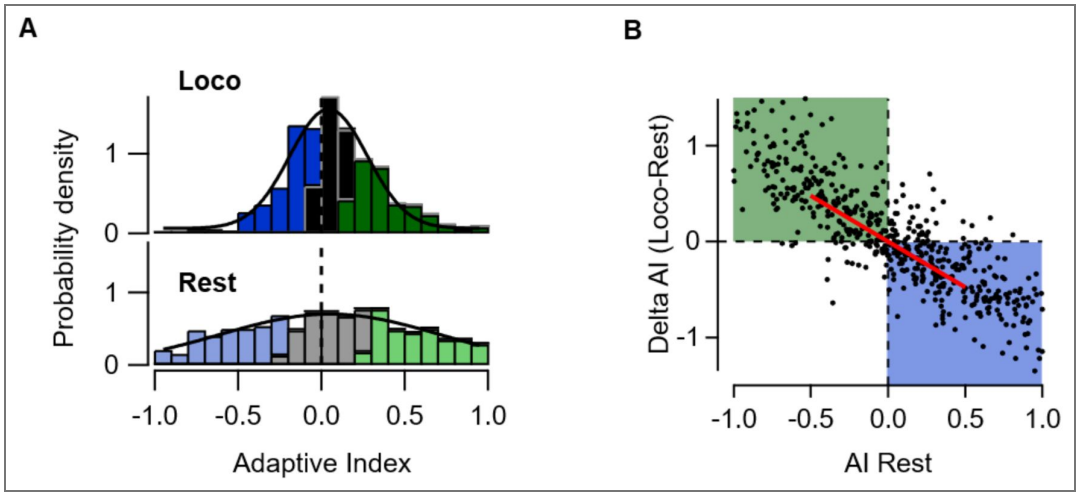

Supplementary Figure 1. Locomotion-dependent changes in adaptive properties of PCs A. The distribution of AIs at rest and during locomotion, reproduced from Fig. 1C. **B.** Scatter plot showing the change in AI as a function of resting AI (each point a single cell; n = 522 neurons, from 9 mice). Cells that depress at rest (AI > 0) rest showed AIs closer to sensitization during locomotion (blue box in lower right quadrant) while cells that sensitize (AI < 0) showed AI closer to depression (green box in upper left quadrant). These shifts in measured AI help explaining the narrowing of the AI distribution in A. The red dashed line is fitted to the data collected from the subset of PCs with AI between -0.5 and 0.5 and reflects a correlation coefficient of r = −0.69.

Similar time-scales of sensitizing and depressing adaptation

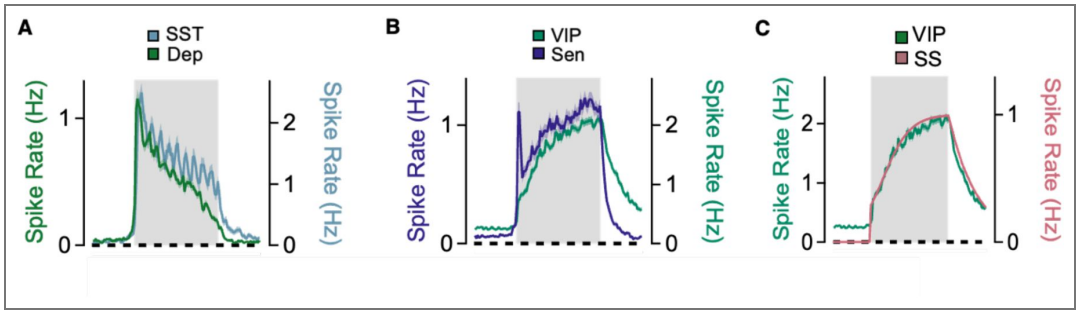

Supplementary Figure 2. Identification of an external signal determining the time-course of slow adaptation. A. Similar dynamics of slow depression in SSTs and the depressing tertile of PCs during locomotion. **B.** Similar dynamics of sensitization in VIPs and the sensitizing tertile of PCs (left axis, blue). **C.** The slow sensitizing input to the model (SS) was based on the average response of the VIP population during locomotion and consists of a step and sigmoid function with a time-constant = 1.71 s (see Fig. 4).

Parameter subspace of valid solutions

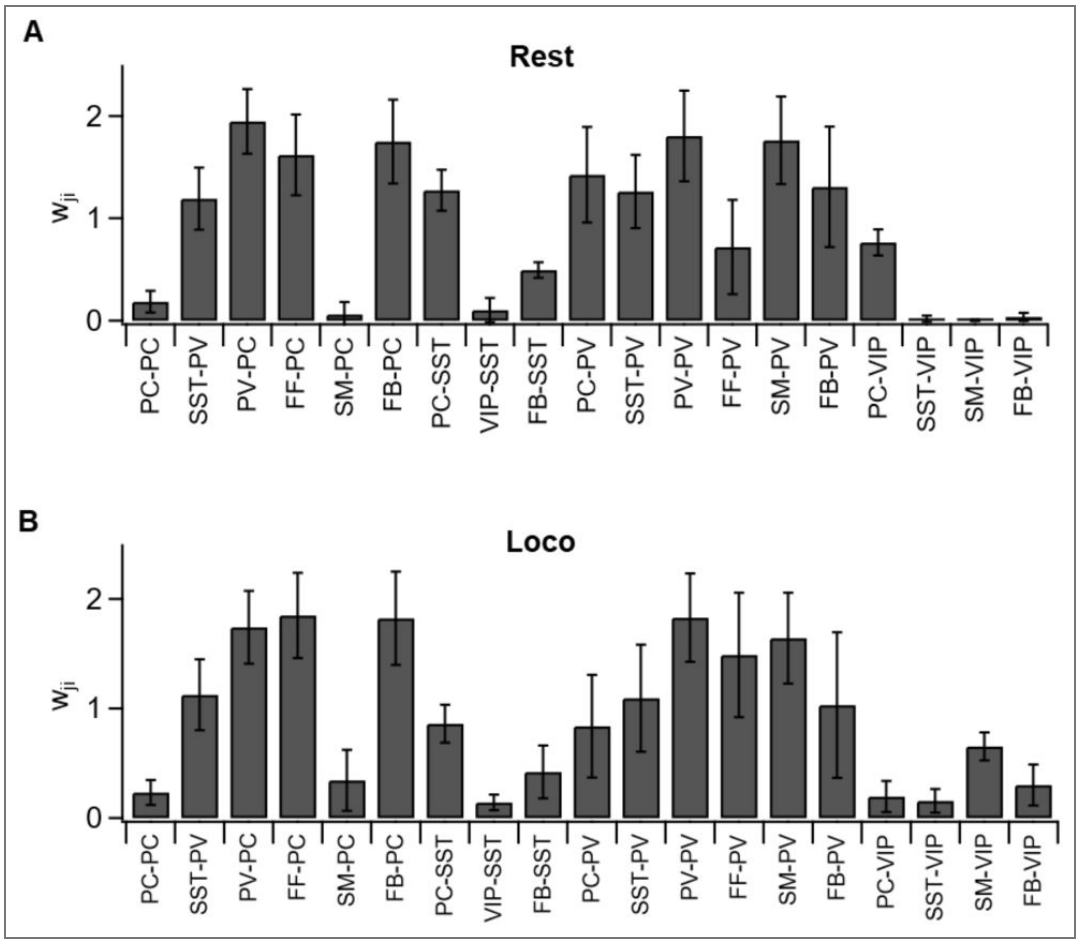

Supplementary Figure 3. A brute force approach delimited a parameter subspace of valid solutions. A. Average connection weights of all the solutions found in the parameter space to give a good fit for the experimental data during rest $(\chi^2_{\text{reduced}} < 3)$. **B.** Average connection weights of all the solutions found in the parameter space to give a good fit for the experimental data during locomotion $(\chi^2_{\text{reduced}} < 10)$

Removing external inputs impairs model performance

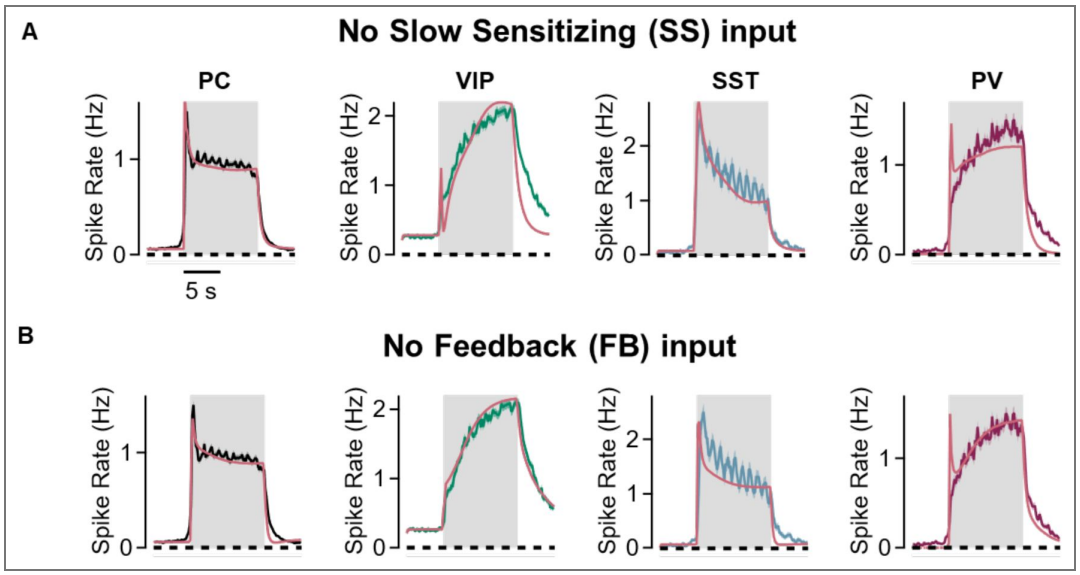

Supplementary Figure 4. Removing external inputs impairs model performance. A. Average firing rates of PCs (black), VIPs (green), SSTs (blue) and PVs (dark red) during stimulus presentation during locomotion and their corresponding fits from the solution with lower (RMSE = 0.14) calculated by a model without slow-sensitizing (SS) input. Note how VIP and PV dynamics are not properly captured. **B.** Same as in A for missing feedback input (FB) (RMSE = 0.14). Note how SST and PV dynamics are not properly captured.

Cell	Total (N, per FOV)	Rest responsive (N, per FOV)	Locomotion responsive (N, per FOV)	Rest responsive only (N, per FOV)	Relative increase during locomotion
PC	78.6 ± 9.4	4.4 ± 1.1	27.8 ± 2.0***	0.5 ± 0.2	6.3 ± 1.7
SST	13.7 ± 1.6	5.1 ± 1.0	6.2 ± 0.7	0.5 ± 0.2	1.2 ± 0.3
PV	32.9 ± 5.4	10.1 ± 2.2	18.4 ± 1.6***	0.3 ± 0.2	1.8 ± 0.4
VIP	53.8 ± 7.2	11.7 ± 6.2	34.9 ± 3.2*	1.3 ± 0.7	3.0 ± 1.6

From left: Total number of cells of each type imaged in a field of view (FOV) of 0.2 mm^2. The number of cells generating a statistically significant response to the stimulus at rest (n = 11, 8, 16, 6 FOVs for PCs, SSTs, PVs and VIPs, respectively) and during locomotion (n = 55, 23, 35, 22). There was a significant increase in the number of responsive PCs and PVs ($p < 0.001$ in both) and VIPs ($p < 0.05$). Locomotion had no significant effect on the number of responsive SSTs. Many fewer cells were responsive at rest but not locomotion, indicating that most cells responsive at rest were also responsive during locomotion. Last column shows the relative change in the number of responsive neurons during locomotion compared to rest.

Supplementary Table 1. Locomotion-associated changes in the number of neurons responding to the visual stimulus

	Rest (Amp in Hz)	**Locomotion** (Amp in Hz)	**Relative Change**[c]
PC	0.57	0.96	0.70
SST	1.52	1.45	-0.05
PV	0.93	1.16	0.25
VIP	0.67	1.63	1.43

Note that activity in external inputs were not directly measured. We therefore kept these constant between rest and locomotion, so that when fitting the model changes in state were reflected only in changes in their connection weights.

Supplementary Table 2. Average response amplitudes in resting and active states

Parameter (text/code)[A]	Description[B]	Value Range[C]	Type[D]	Justification/Source[E]
w_{PC_PC} / w_0	PC to PC population excitatory weight	Min: 0.05 Max: 1.0	Fitted	Known to be less than other local weights[37-39]
W_{FF_PC} / w_1	Feedforward input weight to PC	Min: 0.0 Max: 4.0	Fitted	
W_{SS_PC} / w_2	Slow sensitizing input weight to PC	Min: 0.0 Max: 4.0	Fitted	
W_{PV_PC} / w_3	PV to PC populational inhibitory weight	Min: 0.0 Max: 4.0	Fitted	
W_{SST_PC} / w_4	SST to PC populational inhibitory weight	Min: 0.0 Max: 4.0	Fitted	
W_{PC_PV} / w_5	PC to PV populational excitatory weight	Min: 0.0 Max: 4.0	Fitted	
W_{FF_PV} / w_6	Feedforward input weight to PV	Min: 0.0 Max: 4.0	Fitted	
W_{SS_PV} / w_7	Slow sensitizing input weight to PV	Min: 0.0 Max: 4.0	Fitted	
W_{PV_PV} / w_8	PV to PV populational inhibitory weight	Min: 0.0 Max: 4.0	Fitted	
W_{SST_PV} / w_9	SST to PV populational inhibitory weight	Min: 0.0 Max: 4.0	Fitted	
W_{PC_SST} / w_10	PC to SST populational excitatory weight	Min: 0.0 Max: 4.0	Fitted	
W_{FB_SST} / w_11	Feedback input weight to SST	Min: 0.0 Max: 4.0	Fitted	
W_{VIP_SST} / w_12	VIP to SST populational inhibitory weight	Min: 0.0 Max: 4.0	Fitted	
W_{PC_VIP} / w_13	PC to VIP populational excitatory weight	Min: 0.0 Max: 4.0	Fitted	
W_{SST_VIP} / w_14	SST to VIP populational inhibitory weight	Min: 0.0 Max: 4.0	Fitted	
W_{SS_VIP} / w_15	Slow sensitizing input weight to VIP	Min: 0.0 Max: 4.0	Fitted	
W_{FB_PC} / w_16	Feedback input weight to PC	Min: 0.0 Max: 4.0	Fitted	
W_{FB_PV} / w_17	Feedback input weight to PV	Min: 0.0 Max: 4.0	Fitted	

Supplementary Table 3. **List of parameters used to fit the model**

W_{FB_VIP} / w_18	Feedback input weight to VIP	Min: 0.0 Max: 4.0	Fitted	
τ_{PC} / τ_0	Time constant for PCs	15 ms	Fixed	Experimentally measured in mouse auditory cortex[90]
τ_{VIP} / τ_3	Time constant for VIPs	7.5 ms	Fixed	Experimentally measured in mouse auditory cortex[90]
τ_{PV} / τ_1	Time constant for PVs	19 ms	Fixed	Experimentally measured in mouse auditory cortex[90]
τ_{SST} / τ_2	Time constant for SSTs	19 ms	Fixed	Experimentally measured in mouse auditory cortex[90]
b_{PC} / i_0	Baseline activity of PC cells	Min: 0.0 Hz Max: 0.7 Hz	Fitted	Constant across fittings
b_{PV} / i_1	Baseline activity of PV cells	Min: 0.0 Hz Max: 0.7 Hz	Fitted	Constant across fittings
b_{SST} / i_2	Baseline activity of SST cells	Min: 0.0 Hz Max: 0.7 Hz	Fitted	Constant across fittings
b_{VIP} / i_3	Baseline activity of VIP cells	Min: 0.0 Hz Max: 0.7 Hz	Fitted	Constant across fittings
n / power	Exponent in input-output function (Eq. 6)	2	Fixed	Exponential although linear was also tested[32,86]
A_f / ampl	Initial FF amplitude	1 Hz	Fixed	Fitted to average PC trace
I_0 / base	FF steady-state after fast decay	1 Hz	Fixed	Fitted to average PC trace
λf / decay	FF exponential decay rate	~3.32 s^{-1} (τ=301 ms)	Fixed	Fitted to average PC trace
s_{del} (FF) / delay_1	FF response delay	165 ms	Fixed	Fitted to average PC trace
k / k	Slope of slow FF sensitization	Min: 0.005 Max: 0.15	Fitted	Simplification of L4 data[22,44]
s_k / s_start	Delay when slow FF sensitization starts	184 ms	Fixed	To start after initial peak
$decay_f$ / decay_ff	FF decay time-constant after stimulus end	~2.15 s^{-1} (τ=465 ms)	Fitted	Introduced to fit tails of traces after stimulus representation
A_s / ampl_1	SS sigmoid amplitude	1 Hz	Fixed	Fitted to VIP response and scaled to have average amplitude to be ~1 Hz
λ_s / $\frac{1}{r\_1}$	SS sigmoid rate	~0.58 s^{-1} (r_1=1.71 s)	Fixed	Fitted to VIP response
del / delay_2	SS sigmoid center	1.73 s	Fixed	Fitted to VIP response

Supplementary Table 3. (continued)

$decay_s$ / decay_s	SS decay time-constant after stimulus end	~0.27 s^{-1} (τ=3.7 s)	Fitted	Introduced to fit tails of traces after stimulus representation
A_{fb} /	FB step amplitude	~1 Hz	Fixed	Scaled to have average amplitude ~1 Hz
$S_{fb\ delay}$ / delay_3	FB step delay	370 ms	Fixed	Typical feedback latency[40]. Introduced to fit SST delay
$decay_{fb}$ / decay_f	FB decay time-constant after stimulus end	~0.83 s^{-1} (τ=1.2 s)	Fitted	Introduced to fit tails of traces after stimulus representation

A. Name of the model parameter as presented in the manuscript and in the code (text/code). **B**. Parameter purpose in the text and description. **C**. Parameter value when fixed or range where it was allowed to vary when fitted. **D**. Type of parameter value. Those parameters obtained from the litterature were Fixed, while those that were obtained to fit the data are termed Fitted. **E**. Literature source or data measure used to obtain each parameter.

Supplementary Table 3. (continued)

Data availability

All code and data reported in this paper will be shared by the lead contact upon request. Code and example data sets are available at *https://github.com/lagnadoLab/CortexModel*. Any additional information required to reanalyze the data reported in this manuscript is available from the lead contact upon request.

Acknowledgements

This work was supported by BBSRC grant BB/X009386/1, a PhD scholarship to SD from the Leverhulme Trust (DS-2017-011) and a Researchers at Risk Fellowship to YK from the British Academy and Council for At-Risk Academics (RaR/100503).

Additional information

Funding

Funder	Grant reference number	Author
UKRI | Biotechnology and Biological Sciences Research Council (AFRC)	BB/X009386/1	Leon Lagnado
Leverhulme Trust (The Leverhulme Trust)	DS-2017-011	Sina E Dominiak

References

1. **Wark B.,** Lundstrom B.N., Fairhall A (2007) Sensory adaptation. *Curr Opin Neurobiol* **17**:423-429 https://doi.org/10.1016/j.conb.2007.07.001
2. **Polack P.O.,** Friedman J., Golshani P (2013) Cellular mechanisms of brain state-dependent gain modulation in visual cortex. *Nat Neurosci* **16**:1331-1339 https://doi.org/10.1038/nn.3464
3. **Pakan J.M.,** Lowe S.C., Dylda E., Keemink S.W., Currie S.P., Coutts C.A., Rochefort N.L (2016) Behavioral-state modulation of inhibition is context-dependent and cell type specific in mouse visual cortex. *eLife* **5** https://doi.org/10.7554/eLife.14985
4. **McGinley M.J.,** David S.V., McCormick D.A (2015) Cortical Membrane Potential Signature of Optimal States for Sensory Signal Detection. *Neuron* **87**:179-192 https://doi.org/10.1016/j.neuron.2015.05.038
5. **Lin P.A.,** Asinof S.K., Edwards N.J., Isaacson J.S (2019) Arousal regulates frequency tuning in primary auditory cortex. *Proc Natl Acad Sci U S A* **116**:25304-25310 https://doi.org/10.1073/pnas.1911383116
6. **Adesnik H** (2017) Synaptic Mechanisms of Feature Coding in the Visual Cortex of Awake Mice. *Neuron* **95**:1147-1159.e1144. https://doi.org/10.1016/j.neuron.2017.08.014
7. **Varela J.A.,** Sen K., Gibson J., Fost J., Abbott L.F., Nelson S.B (1997) A Quantitative Description of Short-Term Plasticity at Excitatory Synapses in Layer 2/3 of Rat Primary Visual Cortex. *The Journal of Neuroscience* **17**:7926-7940 https://doi.org/10.1523/JNEUROSCI.17-20-07926.1997
8. **Chance F.S.,** Nelson S.B., Abbott L.F (1998) Synaptic Depression and the Temporal Response Characteristics of V1 Cells. *The Journal of Neuroscience* **18**:4785-4799 https://doi.org/10.1523/JNEUROSCI.18-12-04785.1998
9. **Heintz T.G.,** Hinojosa A.J., Dominiak S.E., Lagnado L (2022) Opposite forms of adaptation in mouse visual cortex are controlled by distinct inhibitory microcircuits. *Nature Communications* **13**:1031 https://doi.org/10.1038/s41467-022-28635-8
10. **Niell C.M.,** Stryker M.P (2010) Modulation of visual responses by behavioral state in mouse visual cortex. *Neuron* **65**:472-479 https://doi.org/10.1016/j.neuron.2010.01.033

11. **Fu Y.,** Tucciarone J.M., Espinosa J.S., Sheng N., Darcy D.P., Nicoll R.A., Huang Z.J., Stryker M.P (2014) A cortical circuit for gain control by behavioral state. *Cell* **156**:1139-1152 https://doi.org/10.1016/j.cell.2014.01.050
12. **Dipoppa M.,** Ranson A., Krumin M., Pachitariu M., Carandini M., Harris K.D (2018) Vision and Locomotion Shape the Interactions between Neuron Types in Mouse Visual Cortex. *Neuron* **98**:602-615.e608. https://doi.org/10.1016/j.neuron.2018.03.037
13. **Goard M.,** Dan Y (2009) Basal forebrain activation enhances cortical coding of natural scenes. *Nat Neurosci* **12**:1444-1449 https://doi.org/10.1038/nn.2402
14. **Pronneke A.,** Scheuer B., Wagener R.J., Mock M., Witte M., Staiger J.F (2015) Characterizing VIP Neurons in the Barrel Cortex of VIPcre/tdTomato Mice Reveals Layer-Specific Differences. *Cereb Cortex* **25**:4854-4868 https://doi.org/10.1093/cercor/bhv202
15. **Lohani S.,** Moberly A.H., Benisty H., Landa B., Jing M., Li Y., Higley M.J., Cardin J.A (2022) Spatiotemporally heterogeneous coordination of cholinergic and neocortical activity. *Nat Neurosci* **25**:1706-1713 https://doi.org/10.1038/s41593-022-01202-6
16. **Kimura F.,** Baughman R.W (1997) Distinct muscarinic receptor subtypes suppress excitatory and inhibitory synaptic responses in cortical neurons. *J Neurophysiol* **77**:709-716 https://doi.org/10.1152/jn.1997.77.2.709
17. **Hasselmo M.E.,** Bower J.M (1992) Cholinergic suppression specific to intrinsic not afferent fiber synapses in rat piriform (olfactory) cortex. *J Neurophysiol* **67**:1222-1229 https://doi.org/10.1152/jn.1992.67.5.1222
18. **Mrzljak L.,** Levey A.I., Goldman-Rakic P.S (1993) Association of m1 and m2 muscarinic receptor proteins with asymmetric synapses in the primate cerebral cortex: morphological evidence for cholinergic modulation of excitatory neurotransmission. *Proc Natl Acad Sci U S A* **90**:5194-5198 https://doi.org/10.1073/pnas.90.11.5194
19. **Haider B.,** Hausser M., Carandini M (2013) Inhibition dominates sensory responses in the awake cortex. *Nature* **493**:97-100 https://doi.org/10.1038/nature11665
20. **Jouhanneau J.S.,** Kremkow J., Dorrn A.L., Poulet J.F (2015) In Vivo Monosynaptic Excitatory Transmission between Layer 2 Cortical Pyramidal Neurons. *Cell Rep* **13**:2098-2106 https://doi.org/10.1016/j.celrep.2015.11.011
21. **Pala A.,** Petersen C.C.H (2015) In vivo measurement of cell-type-specific synaptic connectivity and synaptic transmission in layer 2/3 mouse barrel cortex. *Neuron* **85**:68-75 https://doi.org/10.1016/j.neuron.2014.11.025
22. **Keller A.J.,** Dipoppa M., Roth M.M., Caudill M.S., Ingrosso A., Miller K.D., Scanziani M (2020) A Disinhibitory Circuit for Contextual Modulation in Primary Visual Cortex. *Neuron* **108**:1181-1193.e1188. https://doi.org/10.1016/j.neuron.2020.11.013
23. **Kraynyukova N.,** Renner S., Born G., Bauer Y., Spacek M.A., Tushev G., Busse L., Tchumatchenko T (2022) In vivo extracellular recordings of thalamic and cortical visual responses reveal V1 connectivity rules. *Proc Natl Acad Sci U S A* **119**:e2207032119 https://doi.org/10.1073/pnas.2207032119
24. **Horrocks E.A.B.,** Rodrigues F.R., Saleem A.B (2024) Flexible neural population dynamics govern the speed and stability of sensory encoding in mouse visual cortex. *Nat Commun* **15**:6415 https://doi.org/10.1038/s41467-024-50563-y
25. **Deneux T.,** Kaszas A., Szalay G., Katona G., Lakner T., Grinvald A., Rózsa B., Vanzetta I (2016) Accurate spike estimation from noisy calcium signals for ultrafast three-dimensional imaging of large neuronal populations in vivo. *Nature Communications* **7**:12190 https://doi.org/10.1038/ncomms12190
26. **Friedrich J.,** Zhou P., Paninski L (2017) Fast online deconvolution of calcium imaging data. *PLoS Comput Biol* **13**:e1005423 https://doi.org/10.1371/journal.pcbi.1005423

27. **Rupprecht P.,** Carta S., Hoffmann A., Echizen M., Blot A., Kwan A.C., Dan Y., Hofer S.B., Kitamura K., Helmchen F., *et al.* (2021) A database and deep learning toolbox for noise-optimized, generalized spike inference from calcium imaging. *Nat Neurosci* **24**:1324-1337 https://doi.org/10.1038/s41593-021-00895-5

28. **Berens P.,** Freeman J., Deneux T., Chenkov N., McColgan T., Speiser A., Macke J.H., Turaga S.C., Mineault P., Rupprecht P (2018) Community-based benchmarking improves spike rate inference from two-photon calcium imaging data. *PLoS computational biology* **14**:e1006157 https://doi.org/10.1371/journal.pcbi.1006157

29. **Fairhall A.L.,** Lewen G.D., Bialek W., de Ruyter Van Steveninck R.R. (2001) Efficiency and ambiguity in an adaptive neural code. *Nature* **412**:787-792 https://doi.org/10.1038/35090500

30. **Wilson H.R.,** Cowan J.D (1972) Excitatory and Inhibitory Interactions in Localized Populations of Model Neurons. *Biophysical Journal* **12**:1-24 https://doi.org/10.1016/S0006-3495(72)86068-5

31. **Miller K.D.,** Troyer T.W (2002) Neural Noise Can Explain Expansive, Power-Law Nonlinearities in Neural Response Functions. *Journal of Neurophysiology* **87**:653-659 https://doi.org/10.1152/jn.00425.2001

32. **Rubin Daniel B.,** Van Hooser Stephen D., Miller Kenneth D. (2015) The Stabilized Supralinear Network: A Unifying Circuit Motif Underlying Multi-Input Integration in Sensory Cortex. *Neuron* **85**:402-417 https://doi.org/10.1016/j.neuron.2014.12.026

33. **Pfeffer C.K.,** Xue M., He M., Huang Z.J., Scanziani M (2013) Inhibition of inhibition in visual cortex: the logic of connections between molecularly distinct interneurons. *Nature Neuroscience* **16**:1068-1076 https://doi.org/10.1038/nn.3446

34. **Karnani M.M.,** Jackson J., Ayzenshtat I., Tucciarone J., Manoocheri K., Snider W.G., Yuste R (2016) Cooperative Subnetworks of Molecularly Similar Interneurons in Mouse Neocortex. *Neuron* **90**:86-100 https://doi.org/10.1016/j.neuron.2016.02.037

35. **Brunel N** (2000) Dynamics of sparsely connected networks of excitatory and inhibitory spiking neurons. *J Comput Neurosci* **8**:183-208 https://doi.org/10.1023/a:1008925309027

36. **Deco G.,** Jirsa V.K., Robinson P.A., Breakspear M., Friston K (2008) The dynamic brain: from spiking neurons to neural masses and cortical fields. *PLoS Comput Biol* **4**:e1000092 https://doi.org/10.1371/journal.pcbi.1000092

37. **Jiang X.L.,** Shen S., Cadwell C.R., Berens P., Sinz F., Ecker A.S., Patel S., Tolias A.S (2015) Principles of connectivity among morphologically defined cell types in adult neocortex. *Science* **350**:aac9462 https://doi.org/10.1126/science.aac9462

38. **Hage T.A.,** Bosma-Moody A., Baker C.A., Kratz M.B., Campagnola L., Jarsky T., Zeng H., Murphy G.J (2022) Synaptic connectivity to L2/3 of primary visual cortex measured by two-photon optogenetic stimulation. *eLife* **11**:e71103 https://doi.org/10.7554/eLife.71103

39. **Campagnola L.,** Seeman S.C., Chartrand T., Kim L., Hoggarth A., Gamlin C., Ito S., Trinh J., Davoudian P., Radaelli C., *et al.* (2022) Local connectivity and synaptic dynamics in mouse and human neocortex. *Science* **375**:eabj5861. https://doi.org/10.1126/science.abj5861

40. **Oh S.W.,** Harris J.A., Ng L., Winslow B., Cain N., Mihalas S., Wang Q., Lau C., Kuan L., Henry A.M., *et al.* (2014) A mesoscale connectome of the mouse brain. *Nature* **508**:207-214 https://doi.org/10.1038/nature13186

41. **Froudarakis E.,** Fahey P.G., Reimer J., Smirnakis S.M., Tehovnik E.J., Tolias A.S (2019) The Visual Cortex in Context. *Annu Rev Vis Sci* **5**:317-339 https://doi.org/10.1146/annurev-vision-091517-034407

42. **Roelfsema P.R.,** Lamme V.A., Spekreijse H (1998) Object-based attention in the primary visual cortex of the macaque monkey. *Nature* **395**:376-381 https://doi.org/10.1038/26475

43. **Leinweber M.,** Ward D.R., Sobczak J.M., Attinger A., Keller G.B (2017) A Sensorimotor Circuit in Mouse Cortex for Visual Flow Predictions. *Neuron* **96**:1204 https://doi.org/10.1016/j.neuron.2017.11.009

44. **Makino H.,** Komiyama T (2015) Learning enhances the relative impact of top-down processing in the visual cortex. *Nature Neuroscience* **18**:1116-1122 https://doi.org/10.1038/nn.4061

45. **Fiser A.,** Mahringer D., Oyibo H.K., Petersen A.V., Leinweber M., Keller G.B (2016) Experience-dependent spatial expectations in mouse visual cortex. *Nat Neurosci* **19**:1658-1664 https://doi.org/10.1038/nn.4385

46. **Zhang S.,** Xu M., Kamigaki T., Hoang Do J.P., Chang W.-C., Jenvay S., Miyamichi K., Luo L., Dan Y (2014) Long-range and local circuits for top-down modulation of visual cortex processing. *Science* **345**:660-665 https://doi.org/10.1126/science.1254126

47. **Jin M.,** Glickfeld L.L (2020) Mouse Higher Visual Areas Provide Both Distributed and Specialized Contributions to Visually Guided Behaviors. *Curr Biol* **30**:4682-4692.e4687. https://doi.org/10.1016/j.cub.2020.09.015

48. **Adesnik H.,** Bruns W., Taniguchi H., Huang Z.J., Scanziani M (2012) A neural circuit for spatial summation in visual cortex. *Nature* **490**:226-231 https://doi.org/10.1038/nature11526

49. **Keller G.B.,** Mrsic-Flogel T.D (2018) Predictive Processing: A Canonical Cortical Computation. *Neuron* **100**:424-435 https://doi.org/10.1016/j.neuron.2018.10.003

50. **Shen S.,** Jiang X., Scala F., Fu J., Fahey P., Kobak D., Tan Z., Zhou N., Reimer J., Sinz F., *et al.* (2022) Distinct organization of two cortico-cortical feedback pathways. *Nat Commun* **13**:6389 https://doi.org/10.1038/s41467-022-33883-9

51. **Liu Y.,** Zhang J., Jiang Z., Qin M., Xu M., Zhang S., Ma G (2024) Organization of corticocortical and thalamocortical top-down inputs in the primary visual cortex. *Nat Commun* **15**:4495 https://doi.org/10.1038/s41467-024-48924-8

52. **Jordan R.,** Keller G.B (2020) Opposing Influence of Top-down and Bottom-up Input on Excitatory Layer 2/3 Neurons in Mouse Primary Visual Cortex. *Neuron* **108**:1194-1206.e1195. https://doi.org/10.1016/j.neuron.2020.09.024

53. **Zhang S.,** Xu M., Kamigaki T., Hoang Do J.P., Chang W.C., Jenvay S., Miyamichi K., Luo L., Dan Y (2014) Selective attention. Long-range and local circuits for top-down modulation of visual cortex processing. *Science* **345**:660-665 https://doi.org/10.1126/science.1254126

54. **Yogesh B.,** Keller G.B (2024) Cholinergic input to mouse visual cortex signals a movement state and acutely enhances layer 5 responsiveness. *eLife* **12** https://doi.org/10.7554/eLife.89986

55. **Kim E.J.,** Jacobs M.W., Ito-Cole T., Callaway E.M (2016) Improved Monosynaptic Neural Circuit Tracing Using Engineered Rabies Virus Glycoproteins. *Cell Rep* **15**:692-699 https://doi.org/10.1016/j.celrep.2016.03.067

56. **Tennoe S.,** Halnes G., Einevoll G.T (2018) Uncertainpy: A Python Toolbox for Uncertainty Quantification and Sensitivity Analysis in Computational Neuroscience. *Front Neuroinform* **12**:49 https://doi.org/10.3389/fninf.2018.00049

57. **Billeh Y.N.,** Cai B., Gratiy S.L., Dai K., Iyer R., Gouwens N.W., Abbasi-Asl R., Jia X., Siegle J.H., Olsen S.R., *et al.* (2020) Systematic Integration of Structural and Functional Data into Multi-scale Models of Mouse Primary Visual Cortex. *Neuron* **106**:388-403.e318. https://doi.org/10.1016/j.neuron.2020.01.040

58. **Dadarlat M.C.,** Stryker M.P (2017) Locomotion Enhances Neural Encoding of Visual Stimuli in Mouse V1. *J Neurosci* **37**:3764-3775 https://doi.org/10.1523/JNEUROSCI.2728-16.2017

59. **Erisken S.,** Vaiceliunaite A., Jurjut O., Fiorini M., Katzner S., Busse L (2014) Effects of Locomotion Extend throughout the Mouse Early Visual System. *Current Biology* **24**:2899-2907 https://doi.org/10.1016/j.cub.2014.10.045

60. **Wilson N.R.,** Runyan C.A., Wang F.L., Sur M (2012) Division and subtraction by distinct cortical inhibitory networks in vivo. *Nature* **488**:343-348 https://doi.org/10.1038/nature11347

61. **Lee S.-H.,** Kwan A.C., Zhang S., Phoumthipphavong V., Flannery J.G., Masmanidis S.C., Taniguchi H., Huang Z.J., Zhang F., Boyden E.S., *et al.* (2012) Activation of specific interneurons improves V1 feature selectivity and visual perception. *Nature* **488**:379-383 https://doi.org/10.1038/nature11312

62. **Phillips E.A.,** Hasenstaub A.R (2016) Asymmetric effects of activating and inactivating cortical interneurons. *eLife* **5** https://doi.org/10.7554/eLife.18383

63. **Pi H.-J.,** Hangya B., Kvitsiani D., Sanders J.I., Huang Z.J., Kepecs A (2013) Cortical interneurons that specialize in disinhibitory control. *Nature* **503**:521-524 https://doi.org/10.1038/nature12676

64. **Glickfeld L.L.,** Andermann M.L., Bonin V., Reid R.C (2013) Cortico-cortical projections in mouse visual cortex are functionally target specific. *Nat Neurosci* **16**:219-226 https://doi.org/10.1038/nn.3300

65. **Han Y.,** Kebschull J.M., Campbell R.A.A., Cowan D., Imhof F., Zador A.M., Mrsic-Flogel T.D (2018) The logic of single-cell projections from visual cortex. *Nature* **556**:51-56 https://doi.org/10.1038/nature26159

66. **Ballinger E.C.,** Ananth M., Talmage D.A., Role L.W (2016) Basal Forebrain Cholinergic Circuits and Signaling in Cognition and Cognitive Decline. *Neuron* **91**:1199-1218 https://doi.org/10.1016/j.neuron.2016.09.006

67. **Munoz W.,** Rudy B (2014) Spatiotemporal specificity in cholinergic control of neocortical function. *Curr Opin Neurobiol* **26**:149-160 https://doi.org/10.1016/j.conb.2014.02.015

68. **Gil Z.,** Connors B.W., Amitai Y (1997) Differential regulation of neocortical synapses by neuromodulators and activity. *Neuron* **19**:679-686 https://doi.org/10.1016/s0896-6273(00)80380-3

69. **Xiang Z.,** Huguenard J.R., Prince D.A (1998) GABAA receptor-mediated currents in interneurons and pyramidal cells of rat visual cortex. *J Physiol* **506**:715-730 https://doi.org/10.1111/j.1469-7793.1998.715bv.x

70. **Kruglikov I.,** Rudy B (2008) Perisomatic GABA release and thalamocortical integration onto neocortical excitatory cells are regulated by neuromodulators. *Neuron* **58**:911-924 https://doi.org/10.1016/j.neuron.2008.04.024

71. **Urban-Ciecko J.,** Barth A.L (2016) Somatostatin-expressing neurons in cortical networks. *Nat Rev Neurosci* **17**:401-409 https://doi.org/10.1038/nrn.2016.53

72. **Chen N.,** Sugihara H., Sur M (2015) An acetylcholine-activated microcircuit drives temporal dynamics of cortical activity. *Nat Neurosci* **18**:892-902 https://doi.org/10.1038/nn.4002

73. **Wang Y.,** Gupta A., Toledo-Rodriguez M., Wu C.Z., Markram H (2002) Anatomical, physiological, molecular and circuit properties of nest basket cells in the developing somatosensory cortex. *Cereb Cortex* **12**:395-410 https://doi.org/10.1093/cercor/12.4.395

74. **Silberberg G.,** Markram H (2007) Disynaptic inhibition between neocortical pyramidal cells mediated by Martinotti cells. *Neuron* **53**:735-746 https://doi.org/10.1016/j.neuron.2007.02.012

75. **Muñoz W.,** Tremblay R., Levenstein D., Rudy B (2017) Layer-specific modulation of neocortical dendritic inhibition during active wakefulness. *Science* **355**:954-959 https://doi.org/10.1126/science.aag2599

76. **Tremblay R.,** Lee S., Rudy B (2016) GABAergic Interneurons in the Neocortex: From Cellular Properties to Circuits. *Neuron* **91**:260-292 https://doi.org/10.1016/j.neuron.2016.06.033

77. **Atallah B.V.,** Bruns W., Carandini M., Scanziani M (2012) Parvalbumin-expressing interneurons linearly transform cortical responses to visual stimuli. *Neuron* **73**:159-170 https://doi.org/10.1016/j.neuron.2011.12.013

78. **Fino E.,** Yuste R (2011) Dense Inhibitory Connectivity in Neocortex. *Neuron* **69**:1188-1203 https://doi.org/10.1016/j.neuron.2011.02.025

79. **Hofer S.B.,** Ko H., Pichler B., Vogelstein J., Ros H., Zeng H., Lein E., Lesica N.A., Mrsic-Flogel T.D (2011) Differential connectivity and response dynamics of excitatory and inhibitory neurons in visual cortex. *Nature neuroscience* **14**:1045-1052 https://doi.org/10.1038/nn.2876

80. **Rodarie D.,** Verasztó C., Roussel Y., Reimann M., Keller D., Ramaswamy S., Markram H., Gewaltig M.-O (2022) A method to estimate the cellular composition of the mouse brain from heterogeneous datasets. *PLOS Computational Biology* **18**:e1010739 https://doi.org/10.1371/journal.pcbi.1010739

81. **Schneider-Mizell C.M.,** Bodor A.L., Brittain D., Buchanan J., Bumbarger D.J., Elabbady L., Gamlin C., Kapner D., Kinn S., Mahalingam G., *et al.* (2024) Cell-type-specific inhibitory circuitry from a connectomic census of mouse visual cortex. *bioRxiv* https://doi.org/10.1101/2023.01.23.525290

82. **Bennett C.,** Arroyo S., Hestrin S (2013) Subthreshold mechanisms underlying state-dependent modulation of visual responses. *Neuron* **80**:350-357 https://doi.org/10.1016/j.neuron.2013.08.007

83. **Rao R.P.,** Ballard D.H (1999) Predictive coding in the visual cortex: a functional interpretation of some extra-classical receptive-field effects. *Nat Neurosci* **2**:79-87 https://doi.org/10.1038/4580

84. **Peirce J.W** (2007) PsychoPy--Psychophysics software in Python. *J Neurosci Methods* **162**:8-13 https://doi.org/10.1016/j.jneumeth.2006.11.017

85. **Pachitariu M.,** Stringer C., Schröder S., Dipoppa M., Rossi L.F., Carandini M., Harris K.D. (2016) Suite2p: beyond 10,000 neurons with standard two-photon microscopy. *bioRxiv* https://doi.org/10.1101/061507

86. **Kuchibhotla K.V.,** Gill J.V., Lindsay G.W., Papadoyannis E.S., Field R.E., Sten T.A.H., Miller K.D., Froemke R.C (2017) Parallel processing by cortical inhibition enables context-dependent behavior. *Nature Neuroscience* **20**:62-71 https://doi.org/10.1038/nn.4436

87. **Gáspár M.E.,** Polack P.-O., Golshani P., Lengyel M., Orbán G (2019) Representational untangling by the firing rate nonlinearity in V1 simple cells. *eLife* **8**:e43625 https://doi.org/10.7554/eLife.43625

88. **Newville M.,** Stensitzki T., Allen D.B., Ingargiola A. (2014) LMFIT: Non-Linear Least-Square Minimization and Curve-Fitting for Python. Zenodo.

89. **Sobol I.M.,** Levitan Y. L. (1976) The production of points uniformly distributed in a multidimensional.

90. **Seay M.J.,** Natan R.G., Geffen M.N., Buonomano D.V (2020) Differential Short-Term Plasticity of PV and SST Neurons Accounts for Adaptation and Facilitation of Cortical Neurons to Auditory Tones. *J Neurosci* **40**:9224-9235 https://doi.org/10.1523/JNEUROSCI.0686-20.2020

Peer reviews

Reviewer #1 (Public review):

In this manuscript, Hinojosa and colleagues analysed the changes in V1 visual responses induced by locomotion in head-fixed mice using two-photon calcium imaging. The authors observe that locomotion strongly increases the visual responses of V1 excitatory neurons that exhibit sensitizing responses to visual stimuli. Also, there is an increased response in VIP interneurons, and to a lesser extent, PV interneurons and SST interneurons (non-significant). The authors used a model fitted with data presented in the manuscript, as well as previous knowledge on cortical connectivity among different neuron types. The model suggests that the major component of the increased responses during locomotion is an increase in excitatory drive from external inputs (feedforward, feedback and modulatory), most importantly onto VIP interneurons and excitatory neurons. However, the excitatory drive of local excitatory neurons onto other surrounding excitatory and inhibitory cells is reduced.

The manuscript is well presented and represents a valuable analysis of how locomotion modulates the activity of different subtypes of cortical neurons. However, major issues should be addressed to strengthen the results.

Major issues:

(1) Speed and mismatch between locomotion and visual stimulation.

The authors do not clearly describe the definition of locomotion versus the resting state. The speed should, by itself, have an impact on neuronal responses, especially at the onset of locomotion. Several published studies show that the mismatch between a visual stimulus and the speed of the animal induces specific responses in V1, both in excitatory and subtypes of inhibitory neurons. The authors should address these points upfront in the manuscript, since it is likely a major variable explaining their results

(2) Use of deconvolution with MLSpike.

Some results (Figure 2) exclusively depend on the deconvolution of calcium signals into spikes (since the initial peak is not seen in calcium transients). The authors should validate this result either with electrophysiological recordings or with the use of another deconvolution method (e.g. CASCADE), emphasising the limitations of this approach and the limitations of the time resolution of calcium imaging.

(3) The manuscript is centred around a specific increase in visual responses in sensitizing neurons during locomotion, both in the fraction of responsive neurons and response magnitudes.

It is hard to tell whether this difference is due to a greater scaling effect of locomotion, a difference in responses during the resting state, or both. The manuscript should further explore and discuss the differences in responses between sensitizing and depressing neurons, both during the resting state and locomotion. Adding metrics and direct comparisons of the magnitudes of fast responses, slow responses, and time integrals between sensitizing and depressing neurons in resting and locomotion states would help to clarify this. Same for fractions of responsive neurons of each type in each condition. E.g., the slow phase is harder to judge from the plots, but the DeltaF/F integral shown in Figure 1G seems to suggest the difference in response magnitude between sensitizing and depressing neurons is largest in locomotion state, rather than resting state. How do these integrals look for inferred firing rates shown in Figure 2?

(4) There is something counterintuitive about how the changes in inhibition onto sensitizing and depressing neurons during locomotion explain the reported activity changes.

Sensitizers receive reduced SST input and increased PV input during locomotion. If SSTs depress and PVs sensitize (and this is the main reason why sensitizers, which receive dominant input from SSTs sensitize, and vice-versa), how is it possible that this switch does not alter the sensitizing or depressing nature of these neurons' responses in locomotion? Are these changes insufficient to flip the dominant SST-PV drive? Figure 6D-E seems to show there is a flip, at least for sensitizers. How do authors explain this? Do authors think this is related to the narrowing of the adaptive index distribution shown in Figure 1C?

(5) Presentation of the experimental data and the model.

The manuscript introduces the results of interneuron recordings during the description of the model. Similarly, the results of optogenetic manipulations are presented inside the model's description. It would be clearer to present all experimental data first and introduce the model later, fitting it to all experimental evidence previously presented.

https://doi.org/10.7554/eLife.110088.1.sa3

Reviewer #2 (Public review):

This is an interesting paper with important results. The authors, working in V1, have previously, in a 2022 paper, defined sensitizing and depressing excitatory (E) cells as those whose response increases or decreases, respectively, across the 10 seconds of showing a drifting grating stimulus. They showed that sensitizing E cells are dominantly inhibited by SST inhibitory cells, which are dominantly depressing, and that depressing E cells are dominantly inhibited by PV inhibitory cells, which are very largely sensitizing. It's been well established that locomotion greatly increases E-cell firing rates in V1 compared to rest, but much remains to be worked out as to the mechanism. Here, they find that locomotion increases the responses of the sensitizing E cells much more than depressing cells. They develop a model of changes in synaptic weights between rest and locomotion to account for

the changes. One reason that sensitizers are increased more by locomotion than depressors is that PV cells, which more strongly inhibit depressors, have increased firing for locomotion, whereas SST cells, which more strongly inhibit sensitizers, don't change their firing rates with locomotion. However, in the mode,l a complex array of postulated changes in connection strengths is also involved.

I have, though, a number of concerns: with the model, with the lack of proper discussion of connection to some previous works, and with an overall unclear and confusing presentation and certain controls that should be done.

In the model, they postulate that synapses within the 6-cell-type network - sensitizing, intermediate, and depressing E cells, and PV, SST, and VIP I cells - and from three sources of external input to each of the six types all change between rest and locomotion (except that connections between the E cells don't depend on their types). There are a lot of degrees of freedom, and this makes interpretation of the results difficult. I would have liked to have seen more efforts to constrain the degrees of freedom. For example, there seems to be very little difference between the three E cell types in any of the three types of external input received. Why not constrain them all to get the same external input and see if it significantly affects model fit? Or what if synapses from the three types of external input are left unchanged, and only change their strengths between rest and locomotion? How well could this do? During optimization, why not constrain the changes between rest and locomotion, for example, by putting an L1 penalty on the changes or the relative changes, trying to force them to be sparse, and see whether there are roughly equally good fits? And then, if the main changes are in a small set of synapses, can the authors isolate changes to that small set and do roughly equally well? What about looking at the principal components of the weight changes across models, to isolate patterns of change that are most important?

In terms of comparing to previous works, when optogenetic manipulations of SST and PV are done to test various hypotheses, I would like to see some discussion of what is already known from the authors' 2022 paper and what they are adding or testing that wasn't known or tested from that paper. And Dipoppa et al (2018) also found weight changes to account for the difference between rest and locomotion. They were looking at a fixed point of responses of neurons across retinotopic space to stimuli of various sizes with only one E-cell type, whereas they are accounting for trajectories across time considering 3 E-cell subtypes but without variation in stimuli or retinotopic position of neurons, so the efforts are somewhat different, but still, it would be good to see a bit more discussion of what is in agreement or in contradiction in the conclusions.

In terms of presentation and controls, I have many concerns, which include:

(1) The main result is that sensitizers increase their responses with locomotion ~2X (for dF/F) or about 3.5X (for spikes) more than depressors. But there are other differences between sensitizers and depressors, for example sensitizers have smaller initial stimulus responses at rest, and depressors have larger. What if cells were divided into tertiles by initial stimulus response at rest? Would the authors see the same differences in the effects of locomotion? If so, can they establish whether the difference is really attached to the adaptation properties rather than to, for example, the initial responses, for example, by comparing the regression of response increase against AI vs the regression of response increase against initial resting response? And there might be other controls to be done for other features in which sensitizers and depressors differ.

(2) Lines 103 and following: the authors refer to a "second notable change" which is the narrower distribution of adaptive effects, but I think this is trivial. The adaptive index is AI= (R1-R2)/(R1+R2), where R1 is response 0.5-2.5s after stimulus onset and R2 over 8-10s. But if the change is additive, as suggested by the dF/F figures (and I believe the distributions of AI here are based on dF/F measurements) -- adding the same constant to R1 and R2 will shrink

|AI| without changing the sign of AI. So this would seem to just be a signature of a change that is primarily additive rather than multiplicative.

Also, if the authors do decide that they are going to focus on spikes after showing the raw dF/F, then this analysis should be repeated for spikes.

(3) Figure 2, F is supposed to be D minus E, but it doesn't look like it. For example, the initial response under locomotion is very similar in sensitizers and depressors, so the initial difference in F should be small, but it's not; and at rest, depressors initially have larger responses than sensitizers, whereas later depressors have smaller responses than sensitizers, yet the difference at rest is positive at all times. Something seems wrong here.

https://doi.org/10.7554/eLife.110088.1.sa2

Reviewer #3 (Public review):

This study aimed to understand the depressing and sensitizing effects of adaptation in mice visual cortex during different behavioral states: locomotion and stationary. There is an impressive characterisation of the responses in different cortical cell types and with different optogenetic manipulations to the inhibitory populations. These form a very interesting dataset to understand the effects of the state on the circuits and gain insight into the mechanisms. This data is then used to constrain a model of the responses. Unfortunately, the model appears to be too flexible, and it was difficult to interpret the insights gained from the different model fits.

Strengths:

The data is impressive. There is a characterisation of responses of PCs and VIP, SST and PV interneurons. Additionally, there is the characterisation of some responses to specific optogenetic manipulations, VIP inactivation, SST or PV activation or inactivation. These data will help develop a good insight into the system. The principle of using the optigenetic manipulations to constrain model parameters is very interesting.

Weaknesses:

Many of the analyses have some concerns in the methodology used, which we list in detail below. Further, the model used to gain insight into the mechanism appears overly complicated and seems hard to gain clear insights from.

Major concerns:

(1) Key concern is the usage of dF/F signals for all analyses, especially when comparing responses.

1a) Figure 1G: Comparison of sensitisers and depressors. It is important to consider what the baseline rates are when making these comparisons, especially when comparing the degree of effects between different cell types. For example, if baseline rates for sensitizers were overall higher, it would mean the difference in gain of response would be lower, and could affect the results in the opposite direction of what is claimed. One option to account for this would be to z-score the overall responses, using the same normalization for locomotion and rest. We also suggest plotting differences in sensitisers, intermediates, and depressors as a function of firing rate. Matching for firing rate across each PC categorization and calculating delta AI for each matched firing rate bin.

1b) Figure 2A-F: The above is an even more significant issue when it comes to estimating spiking rates. The methods do not state how dF/F is calculated. If these are based on using the pre-stim as the reference, the algorithms for spike rate used might not be appropriate if this

were used. Using pre-stimulus referencing could result in the estimate going into the wrong range in the calculation of the spike rate.

1c) In both cases above, it could be a problem if baseline firing rates are different between cell types, or states (locomotion/stationary). The latter is established to have effects on many cell types measured, and so needs to be accounted for very carefully.

1d) It would be informative to see per-neuron comparison for adaptive indices during rest and locomotion states. This could be visualized using a scatter plot with AI-rest vs. AI-locomotion for Figures 1D- 1F and 2J- 2L.

1e) Are neurons more strongly modulated between locomotion and rest, also more likely to experience a shift in AI indices (i.e. delta AI). Is there a correlation between the change in firing rate between behavioral states and Delta AI (Loco-Rest)? If so, is this present for all neuron subtypes (e.g. VIP, SST, and PV)?

1f) Optogenetic inhibition of VIP neurons on average abolished the slow depressive effects of adaptation in SST (Figure 3). The strength and prevalence of this effect are unclear. Perhaps one can perform a bootstrap control and opto AI indices and calculate whether AI was significantly reduced following optogenetics inhibition, and if so, on average, how likely was this to occur for the recorded SST neurons? This is important in knowing that the average effects (Figure 3D) aren't driven by a portion of SST neurons, especially as this is later used to confirm the region of parameter space and affects the subsequent results in Figure 4.

(2) Statistics for the effects. There is a mention of Liner mixed models, but no information is given on the actual models being used and tested. This is particularly for the case of Figure 1G, where there is a composition of effect sizes between different populations. What precise significance test is being used? Are the stats on paired cells when considering locomotion and rest?

(3) Model parameters: It is acknowledged that there is a large range of parameters that can model the responses effectively, up to 11% of initial conditions. At 9000 initial conditions, this is around 1000. The parameter estimates are then considered as the mean of each parameter. This seems like a strange choice for a few different reasons:

3a) A mean solution might not be one of the solutions. Let's say the parameters range over a large dimensional space. They could occupy non-overlapping / discontinuous subspaces. In that case, the mean parameters do not necessarily fall within the solution subspaces. Therefore, this reduction to means might not be valid.

3b) Compare distributions rather than means. There are multiple distributions of parameters between conditions. All stats should be on the comparison of distributions rather than just the means.

(4) Visualizing weight matrices: It is very challenging to interpret the weight matrices. Furthermore, it appears that the stationary and locomotion conditions fit independently, and given the large parameter spaces, it is even harder to interpret. Can the fitting instead be done by fitting on one and using those at the initial conditions for the other state? Figure 7 shows an initiative cartoon, but it is not clear how the matrices in Figures 5 and 6 lead to the summary shown in Figure 7. It is also not clear why the connections between inhibitory neurons are not shown in Figure 7. One option is to perhaps run some kind of dimensionality deduction on the parameter space to better interpret the data. When showing deltaWeights, was the model initialised with 'Rest' weights and allowed to change? It is not obvious what the difference is between 'relative change in connection weights' and 'relative change in synaptic weights'.This needs to be clarified.

4a) Model parameters were reduced differently for locomotion and rest (Figure 4). We suggest evaluating the results for locomotion and rest using the same chi-square value of 3 for both behavioral states (at least in controls).

https://doi.org/10.7554/eLife.110088.1.sa1

Author response:

> ***Public Reviews:***
>
> ***Reviewer #1 (Public review):***
>
> *(1) Speed and mismatch between locomotion and visual stimulation.*
>
> *The authors do not clearly describe the definition of locomotion versus the resting state. The speed should, by itself, have an impact on neuronal responses, especially at the onset of locomotion. Several published studies show that the mismatch between a visual stimulus and the speed of the animal induces specific responses in V1, both in excitatory and subtypes of inhibitory neurons. The authors should address these points upfront in the manuscript, since it is likely a major variable explaining their results.*

We will clarify in the methods that a trial was considered as locomotion when an animal ran at a minimum of 3 cm/s for at least 80% of the 10 s stimulus presentation, and was considered rest when running under 3 cm/s during the same fraction of time. Trials with abrupt changes from locomotion to rest were rare and excluded following these criteria.

Locomotion speed and visuomotor mismatch can influence neuronal responses in V1 but in the large majority of our trials mice either run continuously at a stable speed or remained still

i.e locomotion onsets or offsets did not occur (see Hinojosa et al. 2026 for example running traces). Furthermore, sensitizing and depressing neurons were typically recorded simultaneously within the same field of view, experiencing identical locomotor behaviour. For these reasons, we think it is unlikely that differences in speed or mismatch alone can account for the different increase in amplitude observed between depressors and sensitizers.

To directly address this point and further explore the role of speed on V1 neurons, we will quantify the relationship between running speed and amplitude increase in both PCs and interneurons, and include these analyses in the revised version of the manuscript.

> *(2) Use of deconvolution with MLSpike.*
>
> *Some results (Figure 2) exclusively depend on the deconvolution of calcium signals into spikes (since the initial peak is not seen in calcium transients). The authors should validate this result either with electrophysiological recordings or with the use of another deconvolution method (e.g CASCADE), emphasising the limitations of this approach and the limitations of the time resolution of calcium imaging.*

A similar initial increase in amplitude followed by fast depression has been observed previously with electrophysiological recordings in V1 (Chance et al., 1998; Jin & Glickfeld, 2020; Varela et al., 1997). We will further validate our results using an alternative spike inference method like CASCADE (Rupprecht et al., 2021), as well as expanding on the limitations of our approach.

> *(3) The manuscript is centred around a specific increase in visual responses in sensitizing neurons during locomotion, both in the fraction of responsive neurons and response magnitudes.*

> *It is hard to tell whether this difference is due to a greater scaling effect of locomotion, a difference in responses during the resting state, or both. The manuscript should further explore and discuss the differences in responses between sensitizing and depressing neurons, both during the resting state and locomotion. Adding metrics and direct comparisons of the magnitudes of fast responses, slow responses, and time integrals between sensitizing and depressing neurons in resting and locomotion states would help to clarify this. Same for fractions of responsive neurons of each type in each condition. E.g., the slow phase is harder to judge from the plots, but the DeltaF/F integral shown in Figure 1G seems to suggest the difference in response magnitude between sensitizing and depressing neurons is largest in locomotion state, rather than resting state. How do these integrals look for inferred firing rates shown in Figure 2?*

We will further explore the response dynamics of adaptive types within the locomotion and resting state, highlighting the differences between calcium signals and inferred spikes. We will then include our findings in the new version.

> *(4) There is something counterintuitive about how the changes in inhibition onto sensitizing and depressing neurons during locomotion explain the reported activity changes.*
>
> *Sensitizers receive reduced SST input and increased PV input during locomotion. If SSTs depress and PVs sensitize (and this is the main reason why sensitizers, which receive dominant input from SSTs sensitize, and vice-versa), how is it possible that this switch does not alter the sensitizing or depressing nature of these neurons' responses in locomotion? Are these changes insufficient to flip the dominant SST-PV drive? Figure 6D-E seems to show there is a flip, at least for sensitizers. How do authors explain this? Do authors think this is related to the narrowing of the adaptive index distribution shown in Figure 1C?*

This result is only counterintuitive if we consider exclusively the internal connections within V1. The PV:SST ratio changes from 0.9 during rest, dominated by SST induced sensitization, to 1.2, dominated by PV depression. Although adaptation is strongly driven by the opposing inhibition of PV and SST in PCs during locomotion, its origin is more easily explained by an external input (SS) that targets VIPs, PVs and PCs. As a result, when locomotion increases the drive coming from SS input, it injects a source of sensitization that partly balances the decrease in PV:SST ratio, preventing a switch in their adaptive properties which, although reduced, remain sensitizing. We will include these calculations in the revised version.

> *(5) Presentation of the experimental data and the model.*
>
> *The manuscript introduces the results of interneuron recordings during the description of the model. Similarly, the results of optogenetic manipulations are presented inside the model's description. It would be clearer to present all experimental data first and introduce the model later, fitting it to all experimental evidence previously presented.*

We understand that a clear separation between experimental and modelling results is often preferred in papers that combine these approaches but in our case modelling and experimental data are highly interdependent and we believe that an overlapping presentation make it easier for the reader to appreciate the links. One example is Fig. 2G-L that shows experimental results validating a key feature of the model - the use of average response dynamics for each population of interneuron. Similarly, the results in Fig. 3 validate the use of the VIP response dynamics as the template for the slow modulatory input to layer 2/3. Then the results of optogenetic experiments in Fig. 4 are used to narrow down fits to the model. For these reasons, we have chosen to present experimental results and the model in this more integrated manner.

> ***Reviewer #2 (Public review):***
>
> *In the model, they postulate that synapses within the 6-cell-type network - sensitizing, intermediate, and depressing E cells, and PV, SST, and VIP I cells - and from three sources of external input to each of the six types all change between rest and locomotion (except that connections between the E cells don't depend on their types). There are a lot of degrees of freedom, and this makes interpretation of the results difficult. I would have liked to have seen more efforts to constrain the degrees of freedom. For example, there seems to be very little difference between the three E cell types in any of the three types of external input received. Why not constrain them all to get the same external input and see if it significantly affects model fit? Or what if synapses from the three types of external input are left unchanged, and only change their strengths between rest and locomotion? How well could this do? During optimization, why not constrain the changes between rest and locomotion, for example, by putting an L1 penalty on the changes or the relative changes, trying to force them to be sparse, and see whether there are roughly equally good fits? And then, if the main changes are in a small set of synapses, can the authors isolate changes to that small set and do roughly equally well? What about looking at the principal components of the weight changes across models, to isolate patterns of change that are most important?*

To reduce the number of degrees of freedom and ease interpretation we did limit the model fitting for adaptive subtypes by fixing the PC-PC (w_{PC_PC}) and restricting the external inputs weights (w_{FF_PC}, w_{SS_PC}, w_{FB_PC}) to changes of ± 10 %. We will explicitly explain these constrains in the methods and discuss its limitations.

We thank the reviewer for their suggestions of testing different conditions to find those providing the best fit for sensitizing and depressing PCs. We tried an approach similar to that described by Dipoppa et al. 2018 by using the locomotion weights as initial conditions for the rest traces and introducing penalties at later stages. However, the local optimization algorithms failed to reach distant regions of parameter space containing minimum χ^2_{reduced} solutions for the rest condition. We finally opted for repeating the same process of initial condition searching for locomotion and rest, making the L1 penalty approach impracticable in our case. We believe this approach is effective because it has both allowed us to describe circuit changes during internal-state transitions (the present paper) and, more recently, it has made a series of predictions about different learning states that have been confirmed by optogenetic tests (Hinojosa et al., 2026). We will nevertheless explore this and other of the reviewer suggestions to further optimize the fitting in the revised manuscript.

> *In terms of comparing to previous works, when optogenetic manipulations of SST and PV are done to test various hypotheses, I would like to see some discussion of what is already known from the authors' 2022 paper and what they are adding or testing that wasn't known or tested from that paper. And Dipoppa et al (2018) also found weight changes to account for the difference between rest and locomotion. They were looking at a fixed point of responses of neurons across retinotopic space to stimuli of various sizes with only one E-cell type, whereas they are accounting for trajectories across time considering 3 E-cell subtypes but without variation in stimuli or retinotopic position of neurons, so the efforts are somewhat different, but still, it would be good to see a bit more discussion of what is in agreement or in contradiction in the conclusions.*

Thanks for this prompt. We will add further discussion of this work in light of the Heintz et al. (2022) and Dipoppa et al. (2018) papers.

> *(1) The main result is that sensitizers increase their responses with locomotion ~2X (for dF/F) or about 3.5X (for spikes) more than depressors. But there are other differences between sensitizers and depressors, for example sensitizers have smaller initial stimulus*

> *responses at rest, and depressors have larger. What if cells were divided into tertiles by initial stimulus response at rest? Would the authors see the same differences in the effects of locomotion? If so, can they establish whether the difference is really attached to the adaptation properties rather than to, for example, the initial responses, for example, by comparing the regression of response increase against AI vs the regression of response increase against initial resting response? And there might be other controls to be done for other features in which sensitizers and depressors differ.*

We will explore the possibility that initial response influences the increase in amplitude. Preliminary data suggest that initial amplitude is higher in depressors than in sensitizers.

> *(2) Lines 103 and following: the authors refer to a "second notable change" which is the narrower distribution of adaptive effects, but I think this is trivial. The adaptive index is AI=(R1-R2)/(R1+R2), where R1 is response 0.5-2.5s after stimulus onset and R2 over 8-10s. But if the change is additive, as suggested by the dF/F figures (and I believe the distributions of AI here are based on dF/F measurements) -- adding the same constant to R1 and R2 will shrink |AI| without changing the sign of AI. So this would seem to just be a signature of a change that is primarily additive rather than multiplicative.*
>
> *Also, if the authors do decide that they are going to focus on spikes after showing the raw dF/F, then this analysis should be repeated for spikes.*

We agree with the reviewer and will change the text accordingly to highlight the additive nature of the change in amplitude. We will also show the analysis with spikes (this shows similar results as the calcium data).

> *(3) Figure 2, F is supposed to be D minus E, but it doesn't look like it. For example, the initial response under locomotion is very similar in sensitizers and depressors, so the initial difference in F should be small, but it's not; and at rest, depressors initially have larger responses than sensitizers, whereas later depressors have smaller responses than sensitizers, yet the difference at rest is positive at all times. Something seems wrong here.*

We apologize for the confusion this has caused. Figure 2F does not represent the difference between sensitizing and depressing PCs from panels D and E. Instead, it shows the time-varying difference between locomotion and rest states of sensitizers (blue, in figure 2D) and depressors (green, in figure 2E). Thus, panel F shows within-population modulation by behavioural state, rather than differences between sensitizing and depressing neurons. We will amend the figure legend and main text to explain this point and avoid misinterpretation.

> ***Reviewer #3 (Public review):***
>
> *(1) Key concern is the usage of dF/F signals for all analyses, especially when comparing responses.*
>
> *(1a) Figure 1G: Comparison of sensitisers and depressors. It is important to consider what the baseline rates are when making these comparisons, especially when comparing the degree of effects between different cell types. For example, if baseline rates for sensitizers were overall higher, it would mean the difference in gain of response would be lower, and could affect the results in the opposite direction of what is claimed. One option to account for this would be to z-score the overall responses, using the same normalization for locomotion and rest. We also suggest plotting differences in sensitisers, intermediates, and depressors as a function of firing rate. Matching for firing rate across each PC categorization and calculating delta AI for each matched firing rate bin.*
>
> *(1b) Figure 2A-F: The above is an even more significant issue when it comes to estimating spiking rates. The methods do not state how dF/F is calculated. If these are based on*

> *using the pre-stim as the reference, the algorithms for spike rate used might not be appropriate if this were used. Using pre-stimulus referencing could result in the estimate going into the wrong range in the calculation of the spike rate.*
>
> *(1c) In both cases above, it could be a problem if baseline firing rates are different between cell types, or states (locomotion/stationary). The latter is established to have effects on many cell types measured, and so needs to be account ted for very carefully.*

The DF/F0 trace was calculated using the mode of the whole trace as F0. While this approach is less sensitive to biases than subtracting the pre-stimulus, it does not consider noise levels like the z-score suggested by the reviewer. We will, therefore, normalize the calcium traces to z-score to further account for changes in the baseline. Spike inference using MLSpike, however, explicitly models baseline noise and subtracts its effect from that of the spikes calculated from the calcium signal (Deneux et al., 2016). This transformation preserved the difference in amplitude triggered by locomotion between depressing and sensitizing PCs while revealing their similar baseline activity (see Figs. 2D,E and F). These results indicate that the distinct changes in response amplitude between sensitizing and depressing PCs during locomotion are not driven by baseline differences. We will add this explanation to the methods section.

We will also plot the changes in activity with locomotion across cell types as a function of firing rate and add these results to the revised manuscript.

> *(1d) It would be informative to see per-neuron comparison for adaptive indices during rest and locomotion states. This could be visualized using a scatter plot with AI-rest vs. AI-locomotion for Figures 1D- 1F and 2J- 2L.*
>
> *(1e) Are neurons more strongly modulated between locomotion and rest, also more likely to experience a shift in AI indices (i.e. delta AI). Is there a correlation between the change in firing rate between behavioral states and Delta AI (Loco-Rest)? If so, is this present for all neuron subtypes (e.g. VIP, SST, and PV)?*

Sorting was carried out separately on locomotion and rest data sets to capture the adaptive properties of the network under each condition. When assessing the change in adaptive index in individual cells there was a weak but significant correlation ($r = 0.10$, $p<0.05$), probably due to trial to trial stochasticity in the network which has been shown to be present in V1 (Carandini, 2004; Lee et al., 2010). Although adaptation profiles of individual PCs are not fully conserved across rest and locomotion, the observed overlap exceeds that expected by chance, suggesting that stochastic fluctuations modulate an underlying, stable circuit organization. Despite including the stochastic component of the responses, the conclusions hold: sensitizers undergo a larger gain modulation than that of depressors. We will include this analysis and the correlation between change in firing rate and Delta AI in the revised version of the paper.

> *(1f) Optogenetic inhibition of VIP neurons on average abolished the slow depressive effects of adaptation in SST (Figure 3). The strength and prevalence of this effect are unclear. Perhaps one can perform a bootstrap control and opto AI indices and calculate whether AI was significantly reduced following optogenetics inhibition, and if so, on average, how likely was this to occur for the recorded SST neurons? This is important in knowing that the average effects (Figure 3D) aren't driven by a portion of SST neurons, especially as this is later used to confirm the region of parameter space and affects the subsequent results in Figure 4.*

The strength and prevalence of the effect are reflected in the distribution of AI changes across SST neurons, which is centred at $AI = -0.3 \pm 0.3$, indicating a consistent reduction in AI across the population instead of being driven by a small portion of SST neurons. To further

clarify this, we will report the proportion of SST neurons showing a reduction in AI and include statistical analyses on the changes.

> *(2) Statistics for the effects. There is a mention of Liner mixed models, but no information is given on the actual models being used and tested. This is particularly for the case of Figure 1G, where there is a composition of effect sizes between different populations. What precise significance test is being used? Are the stats on paired cells when considering locomotion and rest?*

We used Linear mixed models to test for statistical significance between different conditions composed of hundreds of cells from several mice, i.e. nested analysis (cells nested within mice; see (Judd et al., 2017)). For analyses such as Fig. 1G, we considered locomotion state, adaptive type and their interaction (loco'adap) as fixed effects and mouse number as the random effect. The p-values depicted in the legend indicates the interaction between locomotion and adaptive type, i.e. the increase in amplitude during locomotion is significantly different in sensitizers compared to depressors with $p < 0.0001$. We will revise the method section and figure legends to explicitly describe the model and statistical test used.

> *(3) Model parameters: It is acknowledged that there is a large range of parameters that can model the responses effectively, up to 11% of initial conditions. At 9000 initial conditions, this is around 1000. The parameter estimates are then considered as the mean of each parameter. This seems like a strange choice for a few different reasons:*
>
> *(3a) A mean solution might not be one of the solutions. Let's say the parameters range over a large dimensional space. They could occupy non-overlapping / discontinuous subspaces. In that case, the mean parameters do not necessarily fall within the solution subspaces. Therefore, this reduction to means might not be valid.*
>
> *(3b) Compare distributions rather than means. There are multiple distributions of parameters between conditions. All stats should be on the comparison of distributions rather than just the means.*

To test for the presence of subsets of solutions grouped around different parameter values we plotted the distribution of each parameter across all the good solutions found. Most of the weights were a gaussian distribution centred around the mean and, most importantly, none of them had two peaks. Furthermore, after computing the mean weight values we plotted the solutions given by them in the model, and it rendered a good fit as shown in the figures. We will include those distributions in the new version and base the overall comparison on these distributions.

> *(4) Visualizing weight matrices: It is very challenging to interpret the weight matrices. Furthermore, it appears that the stationary and locomotion conditions fit independently, and given the large parameter spaces, it is even harder to interpret. Can the fitting instead be done by fitting on one and using those at the initial conditions for the other state? Figure 7 shows an initiative cartoon, but it is not clear how the matrices in Figures 5 and 6 lead to the summary shown in Figure 7. It is also not clear why the connections between inhibitory neurons are not shown in Figure 7. One option is to perhaps run some kind of dimensionality deduction on the parameter space to better interpret the data. When showing deltaWeights, was the model initialised with 'Rest' weights and allowed to change? It is not obvious what the difference is between 'relative change in connection weights' and 'relative change in synaptic weights'.This needs to be clarified.*

Thanks for raising this concern. We will firstly try to make the weight matrices clearer to interpret.

Regarding the fitting of rest and locomotion conditions, we fitted the locomotion traces first and used those solutions as initial conditions for the rest traces. However, this rendered no good solutions as minimums in the parameter space were too far from the initial starting points. We opted, therefore, for repeating the same process of initial condition searching for locomotion and rest. This approach is less biased in satisfying our aim of finding solutions that fit the data and can explain their dynamics, which are different for each condition. We believe this approach is effective, as not only has it allowed us to describe circuit changes during internal-state transitions but has also made a series of predictions under different learning states that were confirmed by optogenetic tests (Hinojosa et al., 2026).

We simplified Fig. 7 for clarity but we will make it more accurate and explain it more in detail in the legend, including connections between interneurons.

Interpreting high-dimensional parameter spaces can be challenging. In this study, we focused on low-dimensional summaries of the parameter space (e.g., average connection weights and their distributions across populations), which revealed consistent and interpretable differences between sensitizing and depressing neurons. Importantly, our conclusions do not rely on individual parameter values, but rather on systematic differences across populations that are robust across solutions. Additionally, we ran clustering analysis and found that there is no parameter that can be removed. We focused, therefore, on the larger and more robust differences. We will explore additional dimensionality reduction approaches and include these results if they provide further insight beyond the current analyses.

Finally, the change in weights was calculated with equation 4, in which the weight from locomotion and rest, obtained through independent fits, were used to calculate the relative change from rest to locomotion. These were either connection weights (equation 2) which consider the strength of the connection between cell j and i, or synaptic weights (equation 3) which express the weight of individual synapses by dividing connection weights by the number of presynaptic cells and probability of connection. This distinction arises because we used average traces from all the neurons imaged to fit the model, requiring considering the number of cells to know the strength of individual synapses. We will add this explanation in the results and methods sections.

> *(4a) Model parameters were reduced differently for locomotion and rest (Figure 4). We suggest evaluating the results for locomotion and rest using the same chi-square value of 3 for both behavioral states (at least in controls).*

Thank you for this prompt, this is an important point that we tried to resolve during our analysis. We used the reduced chi-square (χ^2_{reduced}) to evaluate model fits within locomotion and rest condition independently. As defined in equation 12, reduced chi-square is inversely proportional to the standard error of the data which is higher in the rest dataset. As a consequence, setting the same threshold across conditions would not correspond to an equivalent goodness-of-fit criterion, and would impose a disproportionately strict constraint on the condition with lower variability, where deviations between model and data are more heavily penalized. For this reason, we used condition specific χ^2_{reduced} thresholds to ensure comparable fit quality relative to the noise level in each condition. In addition, to enable direct comparison across conditions independent of their noise levels, we used the RMSE as a complementary metric.

References

Carandini, M. (2004). Amplification of trial-to-trial response variability by neurons in visual cortex. PLoS Biol, 2(9), E264. *https://doi.org/10.1371/journal.pbio.0020264*

Chance, F. S., Nelson, S. B., & Abbott, L. F. (1998). Synaptic Depression and the Temporal Response Characteristics of V1 Cells. The Journal of Neuroscience, 18(12), 4785–4799.

https://doi.org/10.1523/JNEUROSCI.18-12-04785.1998

Deneux, T., Kaszas, A., Szalay, G., Katona, G., Lakner, T., Grinvald, A., Rózsa, B., & Vanzetta, I. (2016). Accurate spike estimation from noisy calcium signals for ultrafast three-dimensional imaging of large neuronal populations in vivo. Nature Communications, 7(1), 12190. *https://doi.org/10.1038/ncomms12190*

Dipoppa, M., Ranson, A., Krumin, M., Pachitariu, M., Carandini, M., & Harris, K. D. (2018). Vision and Locomotion Shape the Interactions between Neuron Types in Mouse Visual Cortex. Neuron, 98(3), 602–615.e608. *https://doi.org/10.1016/j.neuron.2018.03.037*

Heintz, T. G., Hinojosa, A. J., Dominiak, S. E., & Lagnado, L. (2022). Opposite forms of adaptation in mouse visual cortex are controlled by distinct inhibitory microcircuits. Nature Communications, 13(1), 1031. *https://doi.org/10.1038/s41467-022-28635-8*

Hinojosa, A. J., Dominiak, S. E., Kosiachkin, Y., & Lagnado, L. (2026). Distinct Disinhibitory Circuits Link Short-Term Adaptation to Familiarity and Reward Learning in Visual Cortex. bioRxiv, 2026.2003.2024.713929. *https://doi.org/10.64898/2026.03.24.713929*

Jin, M., & Glickfeld, L. L. (2020). Magnitude, time course, and specificity of rapid adaptation across mouse visual areas. J Neurophysiol, 124(1), 245–258. *https://doi.org/10.1152/jn.00758.2019*

Judd, C. M., Westfall, J., & Kenny, D. A. (2017). Experiments with More Than One Random Factor: Designs, Analytic Models, and Statistical Power. Annu Rev Psychol, 68, 601–625. *https://doi.org/10.1146/annurev-psych-122414-033702*

Lee, J., Kim, H. R., & Lee, C. (2010). Trial-to-trial variability of spike response of V1 and saccadic response time. J Neurophysiol, 104(5), 2556–2572. *https://doi.org/10.1152/jn.01040.2009*

Rupprecht, P., Carta, S., Hoffmann, A., Echizen, M., Blot, A., Kwan, A. C., Dan, Y., Hofer, S. B., Kitamura, K., Helmchen, F., & Friedrich, R. W. (2021). A database and deep learning toolbox for noise-optimized, generalized spike inference from calcium imaging. Nat Neurosci, 24(9), 1324–1337. *https://doi.org/10.1038/s41593-021-00895-5*

Varela, J. A., Sen, K., Gibson, J., Fost, J., Abbott, L. F., & Nelson, S. B. (1997). A Quantitative Description of Short-Term Plasticity at Excitatory Synapses in Layer 2/3 of Rat Primary Visual Cortex. The Journal of Neuroscience, 17(20), 7926–7940. *https://doi.org/10.1523/JNEUROSCI.17-20-07926.1997*

https://doi.org/10.7554/eLife.110088.1.sa0